UNIVERSITY FOR DEVELOPMENT STUDIES

THE FLOW OF CASSON FLUIDS THROUGH POROUS MEDIA

ABUBAKARI ISSAH

2025

UNIVERSITY FOR DEVELOPMENT STUDIES

THE FLOW OF CASSON FLUIDS THROUGH POROUS MEDIA

BY

ABUBAKARI ISSAH (BED IN MATHEMATICS)

UDS/MMS/0002/23

A THESIS SUBMITTED TO THE FACULTY OF PHYSICAL SCIENCES, DEPARTMENT OF MATHEMATICS IN PARTIAL FULFILLMENT OF THE REQUIREMENTS FOR THE AWARD OF MASTERS OF PHILOSOPHY DEGREE IN MATHEMATICS

AUGUST, 2025

DECLARATION

Student

I hereby declare that this thesis is the result of my original work and that no part of it has been presented for another degree in this University or elsewhere:

Candidate:

Signature:…….. Date: 7th October, 2025

Name: Abubakari Issah

Supervisor

I hereby declare that the preparation and presentation of the thesis was supervised following the guidelines on supervision of thesis laid down by the University for Development Studies.

Supervisor

Signature:…….. Date: Date: 7th October, 2025

Name: Prof. Ibrahim Yakubu Seini

DEDICATION

I dedicate this piece to my mother. and the entire family, who have kindly invested their love and prayers for me to reach this point in my educational journey.

ABSTRACT

This research presents an investigation of a two-dimensional steady flow of an incompressible Casson fluid. The flow is assumed to be in a porous medium with a chemical process and a magnetic field transversely acting on an exponentially stretched surface. The study is significant as the majority of the flow industry exhibits behaviors of a non-Newtonian in nature. The governing equations of the model were derived in the form of partial differential equations, and suitable similarity variables were employed to model the transformation. These produced a coupled form of nonlinear higher-order ordinary differential equations, which were then reduced to a system of first-order ordinary differential equations. The fourth-order Runge–Kutta–Fehlberg method, along with the shooting techniques, was used to obtain numerical solutions using the Maple Software package. Numerical results for the skin friction coefficient, the Nusselt number, and the Sherwood number, which are the most important quantities of interest in engineering practice and give insights into the flow dynamics, were computed and displayed in tables. Graphical results have also been displayed for the model to depict the effects of the controlling parameters on the flow. It was noticed that increases in the Casson parameter caused the skin-friction coefficient to rise, which was accompanied by a decline in the speed of heat and mass transfers. This further resulted in a lower speed of flow along with an enhancement of the thermal boundary layer thickness. The study, therefore, concludes that the use of Casson fluids is crucial in controlling flow kinematics, which are important in achieving desired product characteristics

ACKNOWLEDGEMENT

Praise be to Allah, the universe's God, who has shown his creations unending mercy. I am grateful to Allah Ta'ala for giving me good health to complete my thesis. The existence of the thesis could not have been justified without the benevolence of Allah.

I want to sincerely thank my supervisor, Prof. Ibrahim Yakubu Seini, for his excellent advice and helpful recommendations. His readiness to selflessly donate his valuable time has been much appreciated. Without his valuable assistance, my thesis would not have been possible.

Also, I am grateful to the entire staff of the Physical Sciences Department for their dedication and support.

My deepest gratitude goes to my family, who provide me with the love, prayers, support, and encouragement, and to my best friends.

Thank you.

TABLE OF CONTENTS

Contents

LIST OF TABLES

LIST OF FIGURES

NOMENCLATURE

(u, v)	Velocity components of the field
C_f	Skin friction coefficient
(x, y, z)	Coordinates axes
ρ	Density
p	Pressure
v_o	Injection/suction
T	Temperature (fluid)
T_w	Temperature at the wall
T_∞	Temperature at infinity
C	Concentration (fluid)
C_w	Concentration at the wall
C_∞	Concentration at infinity
u	**V**elocity vector field
U_o	Characteristics velocity
p_y	Yield stress
q_r	Radiative heat flux
B_o	Magnetic field vector
Pr	Prandtl number
Sc	Schmidt number
σ	Electrical conductivity
τ	Skin friction

CHAPTER ONE

INTRODUCTION

1.0 Background of the study

Cason fluids belong to a category of non-Newtonian fluids exhibiting unique flow characteristics influenced by their yield stress and viscosity. In the field of lubrication and biomedical engineering processes, Casson fluids are particularly important. Unlike Newtonian fluids, which assume a linear relationship between the shear stress and shear rate, Casson fluids take into account both the elastic and viscous properties, making them a better approximation of real fluids. Blood, honey, tomato sauce, concentrated fruit juice, paste, and ketchup are examples of Casson fluids. Thus, understanding the behavior of Casson fluid is important for the food processing and packaging industry.

Casson fluids exhibit dual characteristics when subjected to different stresses. It exhibits the properties of solids when the yield stress exceeds the shear stress with infinite viscosity, but behaves like a liquid when the shear stress exceeds the yield stress. Casson fluids are commonly used in polymer processing to control melt flow, extrusion, and moulding processes. The unique rheological properties of Casson fluids make them suitable for coating applications, ensuring even and controlled coating material layers (Chhabra & Richardson, 2011).

In particular, Casson fluids have a significant influence on the flow of lubricants such as heavy oils and greases. They are also used to create sophisticated cooling systems for heat exchangers and electronic components due to their high heat transfer properties (Saidulu & Lakshmi, 2016).

In nanotechnology, Casson fluids are employed in the development of novel materials and devices. In mining and metallurgical processes, it is applied in ore processing, metal casting, and during the flow of nuclear fuel slurries. Akaje (2021) analysed heat and mass transfer flow near

stagnation points in Casson nanofluid on an inclined magnetic field with dissipative viscosity whilst Seini et al. (2020) investigated the Casson fluid boundary layer development on a porous exponentially stretched surface with radiative heat transfer.

The study of Casson fluids has gained traction due to their complex behavior, largely influenced by extrinsic elements like porous materials and magnetic fields. Casson (1959) discussed the rheology of systems in dispersion, such as the flow equation for printing ink-type pigment-oil suspensions. These investigations are crucial for understanding non-Newtonian fluid mechanics to enhance the performance of engineering systems utilizing such fluids.

1.1 Newtonian Fluids

Newtonian fluids are a category of fluids that obey Newton's law of constant viscosity. At shear stress, these fluids exhibit zero shear rate and constant viscosity. Fluids' viscosity is constant regardless of the applied shear rate because the shear stress and shear rate have a linear relationship (Franco & Partal, 2010). Newtonian fluids are mainly characterized by constant viscosity values for a given fixed pressure and temperature condition. Examples of such fluids are water, air, oil, and alcohol.

1.2 Non-Newtonian Fluids

Newton's law of viscosity does not apply to non-Newtonian. They are fluids with variable viscosity that rely on stress. The viscosity of non-Newtonian fluids changes when force applied to it. Shear-independent viscosity in some non-Newtonian fluids still indicates normal stress differences or other non-Newtonian phenomena (Chabra & Richardson, 2011).

1.3 Classes of non-Newtonian fluids

- **Shear-Thinning Fluids**: Shear-thinning fluids are also referred to as pseudoplastics. These fluids become less viscous and flow more readily under increased stress. Paint and ketchup are two examples that flow more easily when squeezed or mixed (Nguyen & Nguyen, 2012).

- **Shear-Thickening Fluids:** Shear thickening fluids become more viscous, or stiffer, with increasing stress. A classic example is cornstarch mixed with water (oobleck). When force is applied, it behaves like a solid, but flows like a liquid under low stress (Price, 2012)

- **Thixotropic Fluids:** These are shear-thinning fluids with time-dependent behavior. They thin out when agitated and slowly return to their thicker state once left undisturbed. An example is honey, which becomes easier to pour when stirred (Glicksman, 2020)

- **Rheopectic Fluids:** These fluids are less common and exhibit the opposite behavior of thixotropic fluids. They thicken over time with applied stress, such as some lubricants (Irgens 2014).

- **Bingham Plastics:** These are plastic materials that behave like solids up to some stress levels and begin to flow like liquids. Toothpaste is an example that flows only after being squeezed (Esmaeili, 2022). The figure (1.1) is an example of a Shear-Thickening fluid described by (Seuss ,1949).

Figure 1.1 Oobleck

Considerable knowledge in the area of fluid dynamics and its applications has huge benefits to engineering practitioners. Many researchers have investigated and explored extensively the field of non-Newtonian fluids and their distinguishing rheological properties.

Fluids are generally categorized as fluids with more complex rheological behavior, whose shear rate is based on factors like the shearing duration and the material history, and fluids whose shear rate is solely reliant on the shear stress at any point, often time-independent and inelastic. These fluids are referred to as time-dependent fluids and belong to the category of visco-elastic fluids (Rao, 1995).

1.4 Statement of the Problem

Understanding the flow behavior of Casson fluids through porous media remains a significant challenge due to their complex non-Newtonian characteristics and interactions with external forces. Despite extensive research on Casson fluid dynamics, limited attention has been given to their behavior under the combined influence of magnetic fields, chemical reactions, and thermal

radiation over exponentially stretching porous surfaces. This gap limits accurate modeling of heat and mass transfer processes essential in biomedical, industrial, and engineering applications. Therefore, this study seeks to develop and analyze a mathematical model for Casson fluid flow through porous media in the presence of a transverse magnetic field, chemical reaction, and thermal radiation to understand their combined effects on velocity, temperature, and concentration distributions.

Research questions

1. How can the flow of Casson fluid through a porous exponentially stretching surface be mathematically modeled in the presence of a magnetic field, thermal radiation, and chemical reaction?
2. What numerical technique can be used to obtain accurate solutions and analyze the Casson fluid flow under the combined effects of magnetic field, radiation, and chemical reaction?
3. How do variations in key flow parameters influence the velocity, temperature, concentration profiles, and related transport characteristics of the Casson fluid?

1.5 Aim and Objectives of the Research

1.5.1 Aim of Study

The aim of this research is to theoretically examine how the Casson fluid behaves when it passes through porous media while a transverse magnetic field is present with reactive substances.

1.5.2 The Research Specific Objectives

The specific objectives of the research are:

1. To formulate a mathematical model of a Casson fluid in the presence of a transverse magnetic field and reactive substances.
2. To analyze the flow of Casson fluids through a porous exponentially stretched surface in the presence of a magnetic field and chemical reaction.
3. To determine the effect of the suction parameter in a Casson fluid flow through a porous exponentially stretched surface.

1.6 Significance of the Research

The significance of studying Casson fluids is to promote and optimize industrial applications. Casson fluids are utilized in the pharmaceutical, cosmetic, and food processing operations for product development and manufacturing. The study is also significant as it will aid in the design of medical devices and implants. Therefore, the significance of this research into Casson fluids lies in its applications across medicine, industry, and fundamental research, which drives innovation and scientific advancement. The study will add to the existing literature and serve as reference material for further research.

1.7 The Scope of the Study

The research is confined to two-dimensional steady, laminar, and incompressible Casson fluid flows across a porous medium over an exponentially stretching surface. It is mainly a theoretical investigation using differential equations to model physical problems.

1.8 Thesis Organization.

The thesis is divided into Five Chapters. Chapter One presents the introduction with a background study. The research problem is stated with the objectives. The literature review is presented in

Chapter Two. Chapter Three presents the methodology of deriving the governing equations. In determining the formulation, the boundary conditions, the impacts of radiation, magnetic field, reaction rate, and Casson parameter are considered. Results and discussion are presented in Chapter Four, and conclusion and recommendations are presented in Chapter Five.

CHAPTER TWO
LITERATURE REVIEW

2.0 Introduction.

Non-Newtonian fluids are extensively applied in manufacturing industries. As a result, many researchers have explored the behavior and features of non-Newtonian fluids. Sakiadis (1961) examined the flow on a boundary layer across a continuous solid sheet. Crane (1970) considered flow over a stretching surface. Kumar & Pai (2020) explored Casson fluid flow through a circular porous bearing, demonstrating how the fluid's properties affect its movement through porous structures. According to what they discovered, the fluid-porous interaction medium is critical for applications such as slider bearings, where efficient lubrication is essential.

Ahmadi et al. (2024) explored Casson fluid flow using magnetohydrodynamics through an expanding or contracting channel using a rectangular porous medium. A rectangular porous medium with walls that can expand or shrink was investigated to demonstrate how temperature influences viscosity in a non-Newtonian fluid with Casson characteristics, incompressibility, and electrical conductivity (Farooq et al. 2015). Reddy et al. (2016) studied the hydromagnetic peristaltic flow of Casson fluids in porous channels and revealed factors such as magnetic field intensity and fluid parameters significantly influence the flow characteristics. This research is particularly relevant for applications in crude oil refinement and biomedical devices where precise control over fluid flow is necessary.

The thermal properties of Casson fluids are also of paramount importance, especially in applications involving heat transfer. Seini (2019) investigated the mass and heat transfer from a convectively heated vertical surface along with internal heat generation and chemical reaction whilst Aloliga et al. (2022) examined the Casson fluid flow with convection and radiative boundary conditions over a porous inclined magnetized surface. Talla (2020) explored the

numerical analysis of MHD flow and heat transport on Casson fluids on an exponentially stretching surface.

Faraz et al. (2020) analyzed MHD's effects on the flow of axi-symmetric Casson nanofluid and revealed how Lorentz forces impact the thermal and flow dynamics over unsteady radially stretching sheets. These studies collectively highlight the significant role of magnetic fields in enhancing or diminishing the thermal performance of Casson fluids. Moreover, the interaction of Casson fluids with nanoparticles has garnered attention, particularly in enhancing thermal conductivity and heat transfer efficiency. Khan et al. (2019) provided a framework for analyzing heat transfer processes in nanofluids, which can be applied to Casson fluids, demonstrating the potential for improved thermal management in engineering applications.

Jamshed et al. (2022) utilized a Keller box method to analyze the entropy generation in Casson hybrid nanofluids, indicating the importance of hybrid nanofluids in optimizing thermal systems. Norasia et al. (2023) studied diamond nanofluids and highlighted how these parameters influence fluid behavior in cylindrical surfaces.

Sulemana et al. (2022) analyzed the hydrodynamic boundary layer flow of reactive fluids over exponentially stretching surfaces whilst Pal & Talukdar (2010) investigated the effects of buoyancy and chemical reactions on MHD mixed convection and mass transfer in a porous medium with ohmic heating and thermal radiation, emphasizing how these factors affect the movement of a fluid with electrical conductivity. Hazarika & Konch (2014) analyzed the flow on inclined surfaces with heat generation. They demonstrated that variations in viscosity and thermal properties could alter the heat transfer rates in MHD systems. This is particularly relevant for Casson fluids as their non-Newtonian behavior can lead to complex interactions under varying thermal conditions. Ramana Reddy & Chamkha (2015) provided insights into the chemical

reaction effects on MHD free convection dissipative fluid flow. Their study emphasized the importance of understanding how chemical reactions can influence MHD systems' thermal and flow characteristics, which is particularly pertinent for Casson fluids used in chemical processing applications.

The coupling of MHD effects with chemical reactions can lead to enhanced heat transfer and mass transport phenomena. Dey et al. (2023) investigated energy transfer in a porous medium via the free convection of a radiating MHD nanofluid past a solid sphere. Sushma & Gireesha (2024) focused on a Casson fluid flow across a stretching surface and heat transfer via stagnation point.

Pramanik (2014) investigated heat transmission and Casson fluid past stretching surfaces with exponential porosity when thermal radiation was present. Yashkun et al. (2024) focused on the impact of velocity slip on magnetized Casson nanofluids over shrinking or stretching cylinders, revealing that variations in the Casson fluid parameters can significantly affect the skin friction coefficient and local Nusselt number.

Dang et al. (2021) investigated the numerical analysis of three-dimensional magnetohydrodynamic (MHD) non-Newtonian flow of a free stream flow induced by a permeable stretching surface. Their findings indicate that radiation and dissipative viscous forces significantly influence the flow characteristics, suggesting that these factors must be considered in practical applications.

Leelavathi et al. (2024) investigated MHD Casson fluid flow over an inclined porous surface under stagnation-point conditions. Koka & Ganjikunta (2024) explored the magnetic field effects of a Casson fluid flow across a sheet which is stretching through a porous medium, emphasizing the role of aligned magnetic fields in modifying flow behavior. Mini et al. (2024) examined

chemically dissipative MHD mixed convective flow over inclined stretching sheets and observed the intricate interactions between thermal radiation and non-Newtonian fluid behavior. Uddin et al. (2024) investigated the MHD convective effects of heat sources on the flow of non-Newtonian fluids and noted that the Casson parameter influences both skin friction and local Nusselt number.

Ahmad et al. (2024) investigated the fractal-fractional modeling of magnetohydrodynamic Casson hybrid nanofluids, emphasizing the potential for heat transfer enhancement through the incorporation of nanoparticles. Their results are complemented by the findings of Noor et al. (2024) who studied sodium alginate-based Casson hybrid nanofluids, highlighting the effects of thermophoresis and heat sinks on fluid behavior. Dhlamini et al. (2024) studied micropolar nanofluid flow based on Cattaneo-Christov heat flux with temperature jump, slip, and relaxation effects.

It is observed from the available literature that the boundary layer flow of Casson fluid is critical in manufacturing and engineering, necessitating further research into various aspects of the problem. Therefore, this research seeks to investigate the effects and behavior of Casson fluid flow through porous media in a transverse magnetic field and chemical reaction.

2.1 The Theory of the Boundary Layer

The boundary layer theory describes fluid behavior near solid boundaries, such as the surface of an object in a fluid. Proposed by Prandtl (1905) cited by Liu (2022). It simplifies the equations of flow into two:

- Most of the drag that a body experiences is due to viscosity, which predominates inside the boundary layer.

- Viscosity can be overlooked outside the boundary layer without significantly altering the solution. This significantly reduces the complexity of the entire Navier-Stokes equations, yielding a solution in both regions in a closed form for the flow.

The same theory holds true for water and other fluids with moderate to low viscosities (other than air). In the event that the temperature difference between the bulk fluid and the velocity boundary layer, most heat transfer to and from a body takes place in this region, making it possible to simplify the equations outside of the boundary layer in the flow field (Moktarian & Modi, 1988)

When fluid flows past a solid boundary, a boundary layer is formed. Internal friction (viscosity) causes the fluid particles at the boundary to stick to it, which results in zero velocity, known as a no-slip condition. The velocity of fluid gradually rises when moving away from the wall, creating a thin region, called the boundary layer, where this velocity transition occurs.

2.2 Hydrodynamic Boundary Layer Thickness

The hydrodynamic boundary layer thickness refers to the distance measured perpendicular from a solid boundary where the velocity of fluid reaches 99% of the free stream velocity (Epifanov, 2011). It represents the extent within the flow where the effects of viscosity and fluid-solid interactions are significant. It is used to analyze the characteristics of fluid flow, such as the development of velocity gradients and the formation of flow patterns near the solid surface. The hydrodynamic boundary layer thickness is a vital parameter in understanding the behavior of fluid flow. Initially, the boundary layer is thin near the leading edge of a surface (referred to as the laminar boundary layer) and consists of smooth and ordered flow. However, as the flow continues, it may undergo a transition to a turbulent boundary layer characterized by increased turbulence and mixing.

2.3 Magnetohydrodynamics (MHD)

Magnetohydrodynamics (MHD) deals with the behavior of fluids conducting electrically in the presence of magnetic and electric fields, such as salt water, plasmas, liquids, electrolytes, and metals (Bau, 2022). Principles from both magnetism and fluid dynamics (Figure 2.1) are combined to explain how these fields interact with the motion of conducting fluids, creating complex effects that are used in various fields, such as astrophysics, geophysics, including engineering (Miyan, 2018). The figure (2.1) below illustrates the MHD power generator according to Bera (2020)

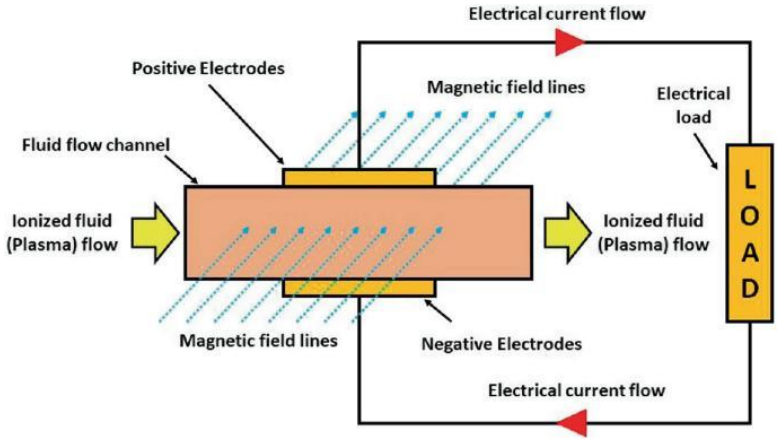

Figure 2.1. MHD power generator

2.4 Transfer of Heat and Mass

The French engineer André Leveque noted in 1928 that only velocity values at the fluid's surface had an impact on convective heat transfer. The heat/mass transition from surface to free-stream heat occurs over a small, narrow area near the surface for flows with high Prandtl numbers. The fluid velocities inside this extremely narrow zone, where the velocity change can be regarded as linear with normal distance from the surface, are therefore the most significant. Heat transfer, which always takes place from a high temperature to a region of lower temperature, is the exchange

of thermal energy between physical systems via dispersing heat, contingent on temperature and pressure gradients. Heat transmission modifies the internal energy of both systems involved, Bergman (2011). Heat transfer can be divided into a number of techniques, such as thermal conduction, convection, radiation, and energy transfer by phase changes. The thermal energy moving as a result of a temperature differential in space is known as heat transfer. Mass transfer is the movement of substances from one location to another due to various forces such as concentration gradient, pressure gradient, or temperature gradient.

2.5. Viscous Dissipation in Flow

The process by which the kinetic energy of a fluid flow is converted into internal thermal energy due to the viscous forces present in the fluid is referred to as viscous dissipation (White & Majdalani, 2006). When fluid layers move at different velocities, friction between them transforms mechanical energy into heat energy, which causes the temperature of the fluid to rise. This effect is especially important when viscosity is high or fluid flows with high-velocity gradients, such as those near solid boundaries or in turbulent flows. Islam et al., (2025) studied Modelling and theoretical overview of Casson fluid flow through a stretching sheet with variable viscosity and sinusoidal boundary conditions.

2.6. Computational Approach

The nonlinear boundary value problem arising from the governing equations was solved numerically using the fourth- order Runge–Kutta–Fehlberg method coupled with the shooting technique. The shooting method transformed the boundary value problem into an initial value problem by iteratively estimating the missing initial conditions until the boundary conditions were satisfied. This combined approach provided high accuracy and stability for solving the coupled nonlinear ordinary differential equations. All computations were implemented using

Maple 2022 software. This numerical procedure is consistent with the methods used by Archana et al. (2018), Sawlat et al. (2024), and Makkar et al. (2023) in analyzing similar nonlinear flow problems.

CHAPTER THREE
DERIVATION AND TRANSFORMATION OF MODEL EQUATIONS

3.0 Introduction

The equations for continuity, momentum, energy, and concentration are developed to investigate the hydrodynamic boundary layer flow of fluid in the form of non-linear partial differential equations. Similar dimensionless variables are used to convert the model into non-linear ordinary differential equations.

3.1 The Continuity Equation

Given in vector form, the continuity equation can be derived from the conservation of mass equation as follows (Clough, 2021).

$$\frac{\partial \rho}{\partial t} + \rho(\nabla . u) = 0 \tag{3.1}$$

$$\frac{\partial \rho}{\partial t} + \frac{\partial(\rho u)}{\partial x} + \frac{\partial(\rho v)}{\partial y} + \frac{\partial(\rho w)}{\partial z} = 0 \tag{3.2}$$

For steady and incompressible flow, equation (3.2) becomes:

$$\frac{\partial u}{\partial x} + \frac{\partial v}{\partial y} + \frac{\partial w}{\partial z} = 0 \tag{3.3}$$

3.2 Equation of momentum

Newton's second law of motion also yields the momentum equation, which is given in a vector form as (Sharma, 2021).

$$\frac{\partial u}{\partial t} + u.\nabla u = -\frac{1}{\rho}p + \mu\nabla^2 u + g \tag{3.4}$$

whereμ is the dynamic viscosity of the fluid, p is the pressure of the fluid, ρ is the density of the fluid, and g is the acceleration due to gravity.

In Cartesian coordinates, including external forces, the equations become;

$$\frac{\partial u}{\partial t}+u\frac{\partial u}{\partial x}+v\frac{\partial u}{\partial y}+w\frac{\partial u}{\partial z}=-\frac{1}{\rho}\frac{\partial p}{\partial x}+\mu\left(\frac{\partial^2 u}{\partial x^2}+\frac{\partial^2 u}{\partial y^2}+\frac{\partial^2 u}{\partial z^2}\right)+g_x+F_x(C,E,B,T) \quad (3.5)$$

$$\frac{\partial v}{\partial t}+u\frac{\partial v}{\partial x}+v\frac{\partial v}{\partial y}+w\frac{\partial v}{\partial z}=-\frac{1}{\rho}\frac{\partial p}{\partial y}+\mu\left(\frac{\partial^2 v}{\partial x^2}+\frac{\partial^2 v}{\partial y^2}+\frac{\partial^2 v}{\partial z^2}\right)+g_y+F_y(C,E,B,T) \quad (3.6)$$

$$\frac{\partial w}{\partial t}+u\frac{\partial w}{\partial x}+v\frac{\partial w}{\partial y}+w\frac{\partial w}{\partial z}=-\frac{1}{\rho}\frac{\partial p}{\partial z}+\mu\left(\frac{\partial^2 w}{\partial x^2}+\frac{\partial^2 w}{\partial y^2}+\frac{\partial^2 w}{\partial z^2}\right)+g_z+F_z(C,E,B,T) \quad (3.7)$$

For a horizontal flow process, the effect of gravity is zero. Since the pressure in a free stream flow is equally distributed in all directions, it is atmospheric and may be disregarded. A reduction of the Navier-Stokes equation follows.

$$\frac{\partial u}{\partial t}+u\frac{\partial u}{\partial x}+v\frac{\partial u}{\partial y}+w\frac{\partial u}{\partial z}=\mu\left(\frac{\partial^2 u}{\partial x^2}+\frac{\partial^2 u}{\partial y^2}+\frac{\partial^2 u}{\partial z^2}\right)+F_x(C,E,B,T) \quad (3.8)$$

$$\frac{\partial v}{\partial t}+u\frac{\partial v}{\partial x}+v\frac{\partial v}{\partial y}+w\frac{\partial v}{\partial z}=\mu\left(\frac{\partial^2 v}{\partial x^2}+\frac{\partial^2 v}{\partial y^2}+\frac{\partial^2 v}{\partial z^2}\right)+F_y(C,E,B,T) \quad (3.9)$$

$$\frac{\partial w}{\partial t}+u\frac{\partial w}{\partial x}+v\frac{\partial w}{\partial y}+w\frac{\partial w}{\partial z}=\mu\left(\frac{\partial^2 w}{\partial x^2}+\frac{\partial^2 w}{\partial y^2}+\frac{\partial^2 w}{\partial z^2}\right)+F_z(C,E,B,T) \quad (3.10)$$

Considering that the flow is predominantly in the x-direction for two-dimensional steady flow with external forces of electric field and magnetic field, resulting in;

$$u\frac{\partial u}{\partial x}+v\frac{\partial u}{\partial y}=\nu\left(\frac{\partial^2 u}{\partial y^2}\right)+F_x(E,B,) \quad (3.11)$$

where $F_x(E, B)$ represent a function of the electric and the magnetic fields.

3.3 The Net Force Model

The net force term in (3.13) depends on E and B which can be modeled for an MHD conducting fluid by assuming a constant magnetic field B_0, electrical conductivity σ, velocity u, and density ρ.

The induced Lorentz force in an MHD by Ohm's law modified for a moving fluid is (Priest, 1982).

$$j = \sigma(\mathrm{E} + \mathrm{u} \times B_0) \tag{3.12}$$

$$\text{If } E = 0,\ j = \sigma(\mathrm{u} \times B_0) \tag{3.13}$$

The Lorentz force per unit volume on a current-carrying fluid is given by

$$f_L = j \times B_0 \tag{3.14}$$

$$f_L = \sigma(\mathrm{u} \times B_0) \times B_0 \tag{3.15}$$

By the use of the cross product, (3.17) becomes

$$fL = \sigma[B_0(u.B_0) - uB_0^2] \tag{3.16}$$

The first term will drop if the velocity is perpendicular to the magnetic field.

Thus, $u.B_0 = 0$, then (3.18) becomes

$$f_L = -\sigma u B_0^2 \tag{3.17}$$

Now, this Lorentz force per unit mass is $\frac{-\sigma u B_0^2}{\rho}$

3.4 Modeling the Casson Fluid

The non-Newtonian fluid with a yield stress is described by the Casson model (Casson, (1959). Its constitutive equation form is;

$$\Gamma = \left(\mu B + \frac{p_y}{\sqrt{2\pi}}\right)\frac{du}{dy}, \text{ for } \Gamma > \Gamma_y \tag{3.18}$$

It is commonly written as an effective viscosity model.

$$\mu_{eff} = \mu\left(1 + \frac{1}{\beta}\right) \tag{3.19}$$

where μ is Newtonian viscosity and β is the Casson parameter

Therefore, the modified term is given as;

$$\mu_{eff} = \nu\left(1 + \frac{1}{\beta}\right) \tag{3.20}$$

3.5 The Energy Equation

The energy equation is derived from the concepts of the principle of energy conservation expressed as (Haugan, 1979)

$$\frac{DT}{Dt} = K\nabla^2 T + G(u, v, w, \mu, T) \tag{3.21}$$

where $K = \frac{\mathrm{K}}{\rho c_p}$ is the thermal diffusivity, c_p is the specific heat capacity at constant pressure, k is the thermal conductivity, and T is the temperature of the fluid. If viscous effects due to temperature variations are not negligible, then the viscous dissipation term, together with radiation and convection effects, can be modeled through G as:

$$G = \frac{\phi}{\rho c_p} + q_{rad} + q_{conv} \tag{3.22}$$

$$\frac{DT}{Dt} = K\nabla^2 T + \frac{\phi}{\rho c_p} + q_{rad} + q_{conv} \tag{3.23}$$

q_{rad} is the radiative heat transfer term where $q_{rad} = \epsilon\sigma(T^4 - T_{evn}^4)$, ϵ is the emissivity, σ is the Stefan-Boltzmann constant, q_{conv} is the convective heat transfer term, where $q_{conv} = h(T - T_{fluid})$, h is the convective heat transfer coefficient.

The convective term is shown on the left side of equation (3.22). On the other hand, the rate at which heat diffuses to the fluid particles is shown on the right-hand side, per unit volume of viscous dissipation, heat loss by radiation, and convection at the boundary. In rectangular steady coordinates, equation (3.23) becomes;

$$u\frac{\partial T}{\partial x} + v\frac{\partial T}{\partial y} + w\frac{\partial T}{\partial z} = \frac{\mathrm{K}}{\rho c_p}\left(\frac{\partial^2 T}{\partial x^2} + \frac{\partial^2 T}{\partial y^2} + \frac{\partial^2 T}{\partial z^2}\right) + 2\mu\frac{1}{\rho c_p}\left(\left(\frac{\partial u}{\partial x}\right)^2 + \left(\frac{\partial v}{\partial y}\right)^2 + \left(\frac{\partial w}{\partial z}\right)^2 + \frac{1}{2}\left(\left(\frac{\partial u}{\partial y} + \frac{\partial v}{\partial x}\right)^2 + \left(\frac{\partial v}{\partial z} + \frac{\partial w}{\partial y}\right)^2 + \left(\frac{\partial w}{\partial x} + \frac{\partial u}{\partial z}\right)^2\right)\right) + \frac{\phi}{\rho c_p} + \epsilon\sigma(T^4 - T_{evn}^4) + h(T - T_{fluid}) \tag{3.24}$$

For two-dimensional steady flow with radiative heat flux contribution and Joule heating (magnetic heating), equation (3.27) reduces to:

$$u\frac{\partial T}{\partial x} + v\frac{\partial T}{\partial y} = \frac{\mathrm{K}}{\rho c_p}\left(\frac{\partial^2 T}{\partial x^2} + \frac{\partial^2 T}{\partial y^2}\right) + \frac{\phi}{\rho c_p} + \epsilon\sigma(T^4 - T_{evn}^4) \quad (3.25)$$

3.6 Magnetic heating model

The dissipative term can be modeled using the power per unit mass dissipated by the Lorentz force

$$P = f_L.u \quad (3.26)$$

$$f_L = \frac{-\sigma u B_0^2}{\rho} \quad (3.27)$$

$$P = \frac{-\sigma B_0^2 u.u}{\rho} \quad (3.28)$$

Since the term represents energy removal, it becomes positive because $u^2 \geq 0$

$$P = \frac{\sigma B_0^2 u^2}{\rho} \quad (3.29)$$

3.7 The Radiative term model

The Rosseland Approximation can be used to model the radiative heat flux in the y-direction (Cess, 1964).

$$q_r = -\frac{4\sigma^*}{3k^*}\frac{\partial T^4}{\partial y} \quad (3.30)$$

where σ^* and k^* are the Stefan-Boltzmann constant and the mean absorption coefficient, respectively. It is assumed that the flow temperature differences are the term T^4 may be expressed

as a linear function of temperature. By Taylor series, T^4 abount T_∞ if expanded and neglecting the higher-order terms leads to:

$$T^4 = T_\infty^4 + 4T_\infty^3(T - T_\infty) \tag{3.31}$$

$$T^4 = 4T_\infty^3 T - 3T_\infty^4 \tag{3.32}$$

$$\frac{\partial T^4}{\partial y} = 4T_\infty^3 \frac{\partial T}{\partial y} \tag{3.33}$$

$$q_r = -\frac{4\sigma^*}{3k^*} .4T_\infty^3 \frac{\partial T}{\partial y} \tag{3.34}$$

$$\frac{\partial q_r}{\partial y} = -\frac{4\sigma^*}{3k^*} .4T_\infty^3 \frac{\partial^2 T}{\partial y^2} \tag{3.35}$$

3.8 The Species Concentration Equation

The general chemical species concentration equation is obtained from Fick's law of mass diffusivity, given as (Cussler, 2009).

$$\frac{DC}{Dt} = D\nabla^2 c + R(T, C, u) \tag{3.36}$$

The model term R can be simplified as;

$$R = \gamma(C - C_\infty), \text{ for } C > C_\infty \tag{3.37}$$

In Cartesian coordinate form as;

$$\frac{\partial C}{\partial t} + \left(u\frac{\partial C}{\partial x} + v\frac{\partial C}{\partial y} + w\frac{\partial C}{\partial z}\right) = D_m\left(\frac{\partial^2 C}{\partial x^2} + \frac{\partial^2 C}{\partial y^2} + \frac{\partial^2 C}{\partial z^2}\right) + \gamma(C - C_\infty) \tag{3.38}$$

3.9. Casson Fluid flow on exponentially stretched porous surface with magnetic and chemical reaction

3.9.1 Modelling the problem

Examine the two-dimensional flow of an incompressible Casson fluid across a porous surface that is exponentially stretching with its origin at $y = 0$. When a uniform magnetic field strength (B_0) is applied transversely to the surface, the flow is restricted to suction. Assuming two equal but opposite forces act to keep the surface stretched with velocity $U = U_w(x) = U_0 e^{\frac{x}{2l}}$ (Figure 3.1).

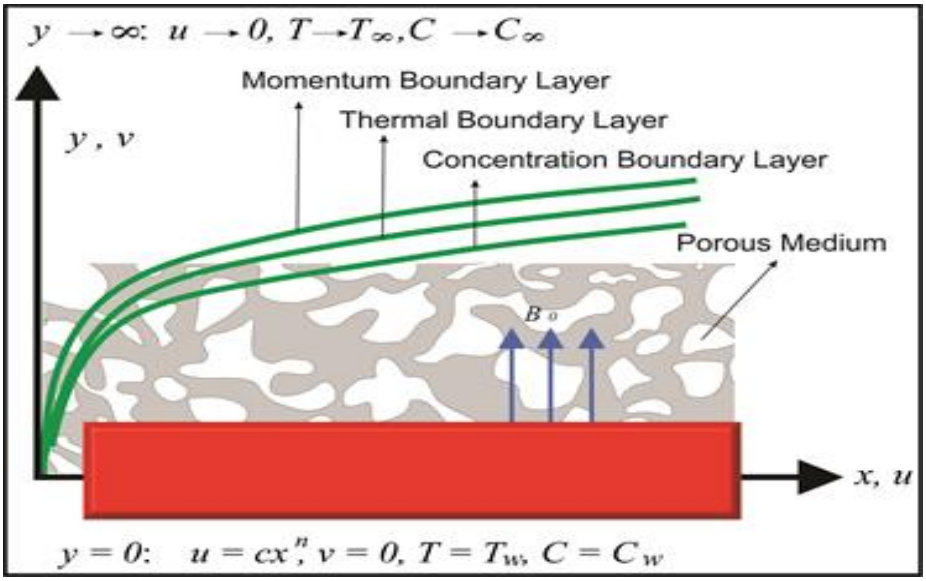

Figure 3.1 Schematic diagram of the problem

For 2-dimensional flow, the continuity equation given in equation (3.3) reduces to:

$$\frac{\partial u}{\partial x} + \frac{\partial v}{\partial y} = 0 \tag{3.39}$$

For a Casson fluid model, if all the relevant terms are substituted, the momentum equation (3.40) becomes;

$$u\frac{\partial u}{\partial x} + v\frac{\partial u}{\partial y} = v\left(1+\frac{1}{\beta}\right)\frac{\partial^2 u}{\partial y^2} - \sigma\frac{B_o^2}{\rho}u \tag{3.41}$$

The energy equation given in equation (3.27) reduces to:

$$u\frac{\partial T}{\partial x} + v\frac{\partial T}{\partial y} = \frac{k}{\rho c_p}\frac{\partial^2 T}{\partial y^2} - \frac{k}{k'}\frac{\partial qr}{\partial y} + \sigma\frac{B_o^2}{\rho}u^2 \tag{3.42}$$

The concentration equation (3.43) becomes;

$$u\frac{\partial C}{\partial x} + v\frac{\partial C}{\partial y} = D\frac{\partial^2 C}{\partial y^2} + \gamma(C - C_\infty) \tag{3.43}$$

The boundary conditions associated with the problem are:

$$u = U_o e^{\frac{x}{2l}}, v = -v_0(x), T = T_w, C = C_w \text{ as } y = 0 \tag{3.44}$$

$$u \to 0,\ T \to T_\infty, C \to C_\infty,\ y \to \infty, \tag{3.45}$$

Here $U = U_o e^{\frac{x}{l}}$ is the stretching velocity.

$T = T_\infty + T_o e^{\frac{x}{2l}}\theta(\eta),\ C = C_\infty + C_o e^{\frac{x}{2l}}\phi(\eta)$ is the temperature and concentration at the sheet.

$U_0,\ T_o, and\ C_0$ are the reference velocity, temperature and concentration respectively.

$V(x) = V_0 e^{\frac{x}{2l}}$ is the velocity at the wall with V_0 as constant.

$V(x) > 0$ is the velocity for suction and $V(x) < 0$ is the velocity for blowing or injection.

3.9.2 Self-Similar Solutions

Blasius (1908) introduced the term 'similarity solution' which is based on the idea that, when displayed in dimensionless form as a function of a precisely defined similarity variable, the

velocity, temperature, and species concentration distributions at each point along the plate surface, x, will collapse. For dimensionless temperature, dimensionless velocity, and dimensionless species concentration, therefore, the partial differential equations that express the issue in terms of x and y will collapse to ordinary differential equations in η.

3.9.3 The Stream Function

The stream function(ψ) is a scalar function used to describe incompressible two-dimensional flow that automatically fulfills the continuity equation. That is:

$$u = \frac{\partial \psi}{\partial y},\ v = -\frac{\partial \psi}{\partial x} \tag{3.46}$$

Assume $\psi(x,y) = \sqrt{2\nu l U_0}\, f(\eta)$ (3.47)

$$\eta = y\sqrt{\frac{U_o}{2\nu l}}e^{\frac{x}{2l}} \tag{3.48}$$

$$u = U_o e^{\frac{x}{l}} f'(\eta),\ v = -\sqrt{\frac{\nu U_o}{2l}}e^{\frac{x}{2l}}[f(\eta) + \eta f'(\eta)] \tag{3.49}$$

3.9.4 The Similarity Variables

Similarity variables are dimensionless combinations of physical variables that aid in transforming partial differential equations to ordinary differential equations (Bluman & Cole, 2012).

$$\eta = y\sqrt{\frac{U_o}{2\nu l}}e^{\frac{x}{2l}},\ u = U_o e^{\frac{x}{l}} f'(\eta),\ v = -\sqrt{\frac{\nu U_o}{2l}}e^{\frac{x}{2l}}[f(\eta) + \eta f'(\eta)] \tag{3.50}$$

$$T = T_\infty + T_o e^{\frac{x}{2l}}\theta(\eta),\quad C = C_\infty + C_o e^{\frac{x}{2l}}\phi(\eta) \tag{3.51}$$

3.9.5 The Dimensionless Continuity Equation.

The continuity equation is automatically satisfied when substituted as follows:

$$\frac{\partial \eta}{\partial x} = \frac{y}{2l}\sqrt{\frac{U_0}{2\nu l}}e^{\frac{x}{2l}}$$

$$\frac{\partial u}{\partial x} = \frac{U_0}{l}e^{\frac{x}{l}}f' + U_0 e^{\frac{x}{l}}f''.\frac{y}{2l}\sqrt{\frac{U_0}{2\nu l}}e^{\frac{x}{2l}} = \frac{U_0}{l}e^{\frac{x}{l}}f' + y\sqrt{\frac{U_0^3}{8\nu l^3}}\ e^{\frac{3x}{2l}}f'' \tag{3.52}$$

Also, $\frac{\partial \eta}{\partial y} = \sqrt{\frac{U_0}{2\nu l}}e^{\frac{x}{2l}}$

$$\frac{\partial v}{\partial y} = -\sqrt{\frac{\nu U_0}{2l}}e^{\frac{x}{2l}}\left(f'.\sqrt{\frac{U_0}{2\nu l}}e^{\frac{x}{2l}} + y\sqrt{\frac{U_0}{2\nu l}}e^{\frac{x}{2l}}f''.\sqrt{\frac{U_0}{2\nu l}}e^{\frac{x}{2l}} + f'.\sqrt{\frac{U_0}{2\nu l}}e^{\frac{x}{2l}}\right)$$

$$= -\frac{U_0}{l}e^{\frac{x}{l}}f' - y\sqrt{\frac{U_0^3}{8\nu l^3}}\ e^{\frac{3x}{2l}}f'' \tag{3.53}$$

Equations (3.51) and (3.52) together satisfied the continuity equation

3.9.6 Dimensionless Momentum equation.

$$\frac{\partial u}{\partial y} = U_0 e^{\frac{x}{l}}f''.\sqrt{\frac{U_0}{2\nu l}}e^{\frac{x}{2l}} = \sqrt{\frac{U_0^3}{2\nu l}}e^{\frac{3x}{2l}}f'' \tag{3.54}$$

$$\frac{\partial^2 u}{\partial y^2} = \sqrt{\frac{U_0^3}{2\nu l}}e^{\frac{3x}{2l}}f'''.\sqrt{\frac{U_0}{2\nu l}}e^{\frac{x}{2l}} = \frac{U_0^2}{2\nu l}e^{\frac{x}{2l}}f''' \tag{3.55}$$

Substitute the relevant terms lead to:

$$U_o e^{\frac{x}{l}}f'\left(\frac{U_0}{l}f'e^{\frac{x}{l}} + y\sqrt{\frac{U_0^3}{8\nu l^3}}\ f''e^{\frac{3x}{2l}}\right) + -\sqrt{\frac{U_o}{2\upsilon l}}e^{\frac{x}{2l}}\left[f + y\sqrt{\frac{U_0}{2\nu l}}e^{\frac{x}{2l}}f'\right]\left(\sqrt{\frac{U_0^3}{2\nu l}}e^{\frac{3x}{2l}}f''\right) = \nu\left(1 +$$

$$\frac{1}{\beta}\right)\frac{U_0^2}{2\nu l}e^{\frac{x}{2l}}f''' - \sigma\frac{B_o^2}{\rho}.U_o e^{\frac{x}{l}}f' \tag{3.56}$$

Expanding and simplifying

$$f'^2 - \frac{1}{2}ff'' = \frac{1}{2}\left(1 + \frac{1}{\beta}\right)f''' - \sigma\frac{lB_o^2}{\rho U_0}.e^{-\frac{x}{l}}f' \tag{3.57}$$

Re-arranging yields:

$$\left(1+\frac{1}{\beta}\right)f''' + ff'' - 2f'^2 - Mf' = 0 \tag{3.58}$$

Where $M = \frac{2l\sigma U_0^2}{\rho U_0 e^{\frac{x}{l}}}$ is the magnetic parameter

.

3.9.7 The equation for dimensionless energy

$$\frac{\partial T}{\partial x} = \frac{T_0}{2l}e^{\frac{x}{2l}}\theta + T_0 e^{\frac{x}{2l}}.y\sqrt{\frac{U_o}{2\nu l}}e^{\frac{x}{2l}}\theta' = \frac{T_0}{2l}e^{\frac{x}{2l}}\theta + \frac{T_0}{2l}y\sqrt{\frac{U_o}{2\nu l}}e^{\frac{x}{l}}\theta' \tag{3.59}$$

$$\frac{\partial T}{\partial y} = T_0 e^{\frac{x}{2l}}\theta'.\sqrt{\frac{U_o}{2\nu l}}e^{\frac{x}{2l}} = T_0 e^{\frac{x}{l}}\sqrt{\frac{U_o}{2\nu l}}\theta' \tag{3.60}$$

$$\frac{\partial^2 T}{\partial y^2} = T_0 e^{\frac{x}{l}}\sqrt{\frac{U_o}{2\nu l}}\theta''.\sqrt{\frac{U_o}{2\nu l}}e^{\frac{x}{2l}} = \frac{T_0 U_0}{2\nu l}e^{\frac{3x}{2l}}\theta'' \tag{3.61}$$

$$\frac{\partial q_r}{\partial y} = -\frac{4\sigma^*}{3k^*}.4T_\infty^3\frac{\partial^2 T}{\partial y^2}$$

Substituting yields

$$U_o e^{\frac{x}{l}}f'\left(\frac{T_0}{2l}e^{\frac{x}{2l}}\theta + \frac{T_0}{2l}y\sqrt{\frac{U_o}{2\nu l}}e^{\frac{x}{l}}\theta'\right) - \sqrt{\frac{U_o}{2\nu l}}e^{\frac{x}{2l}}\left[f + y\sqrt{\frac{U_o}{2\nu l}}e^{\frac{x}{2l}}f'\right]\left(T_0 e^{\frac{x}{l}}\sqrt{\frac{U_o}{2\nu l}}\theta'\right) = k\frac{T_0 U_0}{2\nu l}e^{\frac{3x}{2l}}\theta'' -$$

$$\frac{K}{k'}\frac{4\sigma^*}{3k^*}.4T_\infty^3\frac{T_0 U_0}{2\nu l}e^{\frac{3x}{2l}}\theta'' + \sigma\frac{B_o^2}{\rho}\left(U_o e^{\frac{x}{l}}f'\right)^2$$

$$\frac{T_0 U_0}{2l}e^{\frac{3x}{2l}}f'\theta + \frac{T_0}{2l}e^{\frac{2x}{l}}y\sqrt{\frac{U_0^3}{2\nu l}}f'\theta' - \frac{T_0 U_0}{2l}e^{\frac{3x}{2l}}f\theta' - \frac{T_0}{2l}e^{\frac{2x}{l}}y\sqrt{\frac{U_0^3}{2\nu l}}f'\theta' = k\frac{T_0 U_0}{2\nu l}e^{\frac{3x}{2l}}\theta'' +$$

$$k\frac{16T_0 T_\infty^3 U_0}{k'3k^*2\nu l}e^{\frac{3x}{2l}}\theta'' + \frac{\sigma B_0^2 U_0^2}{\rho}e^{\frac{2x}{l}}f'^2$$

$$\left(1+\frac{4}{3}Ra\right)\theta'' + Prf\theta' - Prf'\theta + MPrEcf'^2 = 0, \tag{3.62}$$

where $M = \frac{2l\sigma B_0^2}{\rho U_0 e^{\frac{x}{l}}}$ is the parameter of the magnetic field, $Ec = \frac{U_0^2}{c_p(T_w - T_\infty)}$, is the Eckert number.

$Ra = \frac{4\sigma^* T^3}{k^* k'}$, is the parameter of thermal radiation, $\Pr = \frac{\upsilon}{k}$ is the Prandtl number.

3.9.8 The dimensionless concentration equation.

$$\frac{\partial C}{\partial x} = \frac{1}{2l} C_0 e^{\frac{x}{2l}} \emptyset + \frac{1}{2l} C_0 y \sqrt{\frac{U_o}{2\upsilon l}} e^{\frac{x}{2l}} . e^{\frac{x}{2l}} \emptyset' = \frac{1}{2l} C_0 \emptyset e^{\frac{x}{2l}} + \frac{1}{2l} C_0 y \sqrt{\frac{U_o}{2\upsilon l}} e^{\frac{x}{l}} \emptyset' \quad (3.63)$$

$$\frac{\partial C}{\partial y} = C_0 e^{\frac{x}{2l}} \emptyset' . \sqrt{\frac{U_o}{2\upsilon l}} e^{\frac{x}{2l}} = C_0 \sqrt{\frac{U_o}{2\upsilon l}} e^{\frac{x}{l}} \emptyset' \quad (3.64)$$

$$\frac{\partial^2 C}{\partial y^2} = C_0 \sqrt{\frac{U_o}{2\upsilon l}} e^{\frac{x}{l}} \emptyset'' . \sqrt{\frac{U_o}{2\upsilon l}} e^{\frac{x}{2l}} = \frac{C_0 U_0}{2\upsilon l} e^{\frac{3x}{2l}} \emptyset'' \quad (3.65)$$

Substituting relevant terms into the concentration equation and simplifying yields:

$$U_o e^{\frac{x}{l}} f' \left(\frac{1}{2l} C_0 e^{\frac{x}{2l}} \emptyset + \frac{1}{2l} y C_0 \sqrt{\frac{U_o}{2\upsilon l}} e^{\frac{x}{l}} \emptyset' \right) + - \sqrt{\frac{U_o}{2\upsilon l}} e^{\frac{x}{2l}} \left[f + y \sqrt{\frac{U_o}{2\upsilon l}} e^{\frac{x}{2l}} f' \right] \left(C_0 \sqrt{\frac{U_o}{2\upsilon l}} e^{\frac{x}{l}} \emptyset' \right) =$$

$$D \frac{C_0 U_0}{2\upsilon l} e^{\frac{3x}{2l}} \emptyset'' + \gamma C_0 e^{\frac{x}{2l}} \emptyset$$

$$\frac{U_0 C_0}{2l} e^{\frac{3x}{2l}} f' \emptyset + \frac{C_0 y}{2l} \sqrt{\frac{U_0^3}{2\upsilon l}} e^{\frac{x}{2l}} f' \emptyset' - \frac{U_0 C_0}{2l} e^{\frac{3x}{2l}} f \emptyset' - \frac{C_0 y}{2l} \sqrt{\frac{U_0^3}{2\upsilon l}} e^{\frac{x}{2l}} f' \emptyset' = D \frac{C_0 U_0}{2\upsilon l} e^{\frac{3x}{2l}} \emptyset'' + \gamma C_0 e^{\frac{x}{2l}} \emptyset$$

$$\phi'' + Scf\phi' - Scf'\phi + Sc\lambda\phi = 0 \quad (3.66)$$

where $Sc = \frac{\nu}{D}$ is the Schmidt numbe of, $\lambda = \frac{2l\gamma}{U_0 e^{\frac{x}{l}}}$ is the reaction rate parameter.

3.9.9 The dimensionless Boundary conditions

When $y = 0, \eta = 0$ and $y = \infty, \eta = \infty$, then

$u = U_0 e^{\frac{x}{l}} f'(0); U_0 e^{\frac{x}{2l}} f'(0) = U_0 e^{\frac{x}{l}}$

$f'(0) = 1$ (3.67)

$v = -\sqrt{\frac{\upsilon U_o}{2l}} e^{\frac{x}{2l}} [f(\eta) + \eta f'(\eta)] = -v_0(x) \quad = \sqrt{\frac{\upsilon U_o}{2l}} e^{\frac{x}{2l}} [f(0) + (0) f'(0)] = v_0(x)$

Where $f(0) = f_w \to S$ for Suction as $\frac{v_0(x)}{\sqrt{\frac{\upsilon U_0}{2l}}}$

$f(0) = f_w$ (3.68)

$T = T_\infty + T_o e^{\frac{x}{2l}} \theta(0), \; T_w = T_\infty + T_o e^{\frac{x}{2l}} \theta(0), T_w - T_\infty = T_o e^{\frac{x}{2l}} \theta(0)$

$\theta(0) = \frac{T_w - T_\infty}{T_o e^{\frac{x}{2l}}}$, But $T_o e^{\frac{x}{2l}} = T_w - T_\infty$

$\theta(0) = \frac{T_w - T_\infty}{T_w - T_\infty}, \theta(0) = 1$ (3.69)

$C = C_\infty + C_o e^{\frac{x}{2l}} \phi(0),$

$\phi(0) = \frac{C_w - C_\infty}{C_0 e^{\frac{x}{2l}}},$ $\phi(0) = \frac{C_w - C_\infty}{C_w - C_\infty} = 1$ (3.70)

$U \to 0, T \to T_\infty, C \to C_\infty$

$u = U_0 e^{\frac{x}{2l}} f'(\infty), 0 = U_0 e^{\frac{x}{2l}} f'(\infty), f'(\infty) \to 0$ (3.71)

$$T = T_\infty + T_o e^{\frac{x}{2l}}\theta(\infty)$$

$$T_\infty - T_\infty = T_o e^{\frac{x}{2l}}\theta(\infty), 0 = T_o e^{\frac{x}{2l}}\theta(\infty), \theta(\infty) \to 0 \quad (3.72)$$

$$C = C_\infty + C_o e^{\frac{x}{2l}}\phi(\infty)$$

$$C_\infty - C_\infty = C_o e^{\frac{x}{2l}}\phi(\infty), 0 = C_o e^{\frac{x}{2l}}\phi(\infty), \phi(\infty) \to 0 \quad (3.73)$$

Therefore, the boundary conditions for equations (3.50) and (3.51) are:

$$f'(0) = 1, f(0) = f_w, f(\infty) = 0, \theta(0) = 1, \theta(\infty) = 0, \phi(0) = 1, \phi(\infty) = 0 \quad (3.74)$$

The most important quantities of practical relevance to engineers are the skin-friction coefficient, the rate of heat transfer (the Nusselt number), and the rate of mass transfer (the Sherwood number), which are respectively defined for Casson fluids (Reddy et al., 2016; Farooq et al., 2015).

$$C_f = (1 + \frac{1}{\beta})\frac{\tau_w}{\rho u_w^2}, \quad \mathrm{Nu_x} = \frac{\mathrm{xq_w}}{\alpha(\mathrm{T_w} - \mathrm{T_\infty})}, \ \mathrm{Sh_x} = \frac{\mathrm{xq_m}}{\mathrm{D_B}(\mathrm{C_w} - \mathrm{C_\infty})} \quad (3.75)$$

where τ_w is the shear stress of the wall, q_w is the heat flux of the wall and q_m is the mass flux of the wall given as:

$$\tau_w = \mu(\frac{\partial u}{\partial y})_{y=0}, q_w = -k\left(\frac{\partial T}{\partial y}\right)_{y=0}, q_m = -D_B\left(\frac{\partial C}{\partial y}\right)_{y=0} \quad (3.76)$$

In dimensionless form:

$$Re_x^{1/2} C_f = \left(1 + \frac{1}{\beta}\right) f"(0), \ Re_x^{-1/2} Nu_x = -\theta'(0), \ Re_x^{-1/2} Sh_x = -\emptyset'(0), \quad (3.77)$$

where, $Re_x = \frac{x}{\upsilon} U_w(x)$ is the local Reynolds number based on the stretching velocity $U_w(x)$

3.10 Numerical Methods and Analysis

A numerical method of shooting techniques and fourth-fifth order Runge-Kutta-Fehlberg method is employed to investigate and solve the above-proposed research problem. The results are presented graphically and numerically using computer software Maple 22, similar to Sawlat et al. (2024).

The dimensionless equations as modelled above are third-order ordinary differential equations. The fourth-fifth order Runge–Kutta–Fehlberg method with the shooting approach is used to solve the reduced form of the system of coupled first-order ordinary differential equations, similar to Archana et al. (2018) by letting:

$$f = x_1,\ f' = x_2,\ f'' = x_3,\ \theta = x_4,\ \theta' = x_5,\ \phi = x_6,\quad \phi' = x_7 \tag{3.78}$$

We obtain $x_1' = f' = x_2,$

$$x_2' = f'' = x_3,$$

$$x_3' = f''' = \frac{1}{(1+\frac{1}{\beta})}\left(2x_2^2 - x_1x_3 + Mx_2\right), \tag{3.79}$$

$$x'_4 = \theta' = x_5$$

$$x_5' = \theta'' = \frac{1}{(1+\frac{4}{3}Ra)}(Prx_2x_5 - Prx_1x_6 - MPrEcx_2^2),$$

$$x'_6 = \phi' = x_7,$$

$$x'_7 = \phi'' = Sc(x_2x_8 - x_1x_9 - \lambda x_8),$$

where differentiation with respect to η is indicated by the symbol ($'$).

The initial conditions are

$$\begin{bmatrix} x_1(0) \\ x_2(0) \\ x_3(0) \\ x_4(0) \\ x_5(0) \\ x_6(0) \\ x_7(0) \end{bmatrix} = \begin{bmatrix} s_1 \\ 1 \\ s_2 \\ 1 \\ 1 \\ s_3 \\ 1 \end{bmatrix} \tag{3.80}$$

The initial guess for the missing values s_1, s_2, s_3 (that is, $f''(0), \theta'(0), \emptyset'(0)$) are selected systematically, and the initial value problem is solved repeatedly with the help of the Runge–Kutta–Fehlberg method. The Newton-Raphson method is used to guess the initial condition values until the circumstances of the boundary at $\eta \to \infty$ are met.

To calculate the approximate value of η_∞ .We start by using the estimated value to solve the equations that make up the problem. The larger value of η_∞ is used to repeat this process until the difference between successive values of the boundary conditions that are missing for η_∞ differs only in the necessary significant figures. The final numerical value, η_∞ follows. For a given collection of embedded parameters, it is assumed to be the approximate value of η_∞

For this study, we take $\eta_\infty = 10$, and hence, $f'(\infty) = 0$, $\theta(\infty) = 0$, and $\emptyset(\infty) = 0$ become $f'(10) = 0$, $\theta(10) = 0$, and $\emptyset(10) = 0$. Therefore, the choice of $\eta_\infty = 10$ verifies that every numerical solution precisely approached the asymptotic values. The computational solutions for the transformed problem are obtained using the MAPLE software tools. The step size that is utilized in each computation is $\triangle\eta = 0.001$ for a convergence criterion of 10^{-6} for all cases. The highest value of $\eta \to \infty$ to each parameter when the last loop has an inaccuracy of no more than 10^{-6} and the conditions of the unknown boundary values stay the same.

Figure (3.2) is the flow chart illustrating the method. According to Makkar et al. (2023)

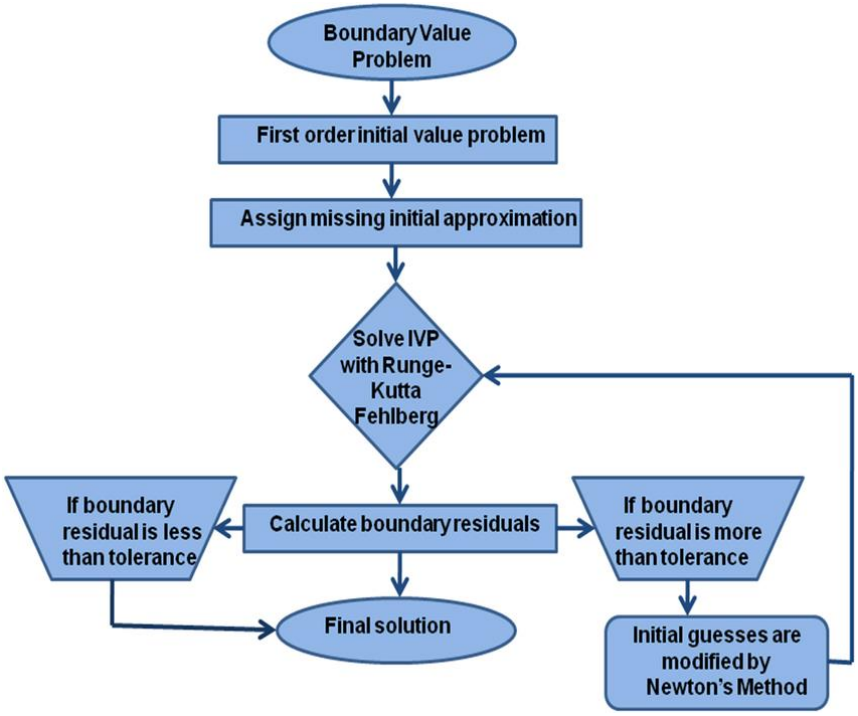

Figure 3.2

CHAPTER FOUR
RESULTS AND DISCUSSIONS

4.0 Introduction

The results of the research are presented in this chapter. Numerical comparison is made with Talla (2020) for the skin-friction coefficient, $f''(0)$ and the local Nusselt number, $-\theta'(0)$ when $\lambda = 0, Ec = 0, Sc = 0$ and $Ra = 0$. A perfect agreement can be seen in Table 4.1 to validate the computational method employed.

Table 4.1. Comparisons of results for $-f''(0)$ and $-\theta'(0)$ with Talla (2020)

Talla (2020)						Present Study					
Pr	B	M	S	$-\theta'(0)$	$-f''(0)$	Pr	B	M	S	$-\theta'(0)$	$-f''(0)$
0.71	0.5	1.0	0.1	0.8696	0.9567	0.71	0.5	1.0	0.1	0.8696	0.9567
0.71	1.0	1.0	0.1	0.8187	1.1762	0.71	1.0	1.0	0.1	0.8187	1.1762
0.71	1.5	1.0	0.1	0.7929	1.2910	0.71	1.5	1.0	0.1	0.7929	1.2910
2.00	0.5	1.0	0.1	1.6647	0.9567	2.00	0.5	1.0	0.1	1.6647	0.9567
5.00	0.5	1.0	0.1	2.8775	0.9567	5.00	0.5	1.0	0.1	2.8775	0.9567
7.10	0.5	1.0	0.1	3.5431	0.9567	7.10	0.5	1.0	0.1	3.5431	0.9567
0.71	0.5	1.5	0.1	0.8476	1.0419	0.71	0.5	1.5	0.1	0.8476	1.0419
0.71	0.5	2.0	0.1	0.8276	1.1205	0.71	0.5	2.0	0.1	0.8276	1.1205
0.71	0.5	2.5	0.1	0.8092	1.1937	0.71	0.5	2.5	0.1	0.8092	1.1937
0.71	0.5	1.0	0.2	0.9128	0.9731	0.71	0.5	1.0	0.2	0.9128	0.9731
0.71	0.5	1.0	0.3	0.9573	0.9898	0.71	0.5	1.0	0.3	0.9573	0.9898
0.71	0.5	1.0	0.4	1.0030	1.0068	0.71	0.5	1.0	0.4	1.0030	1.0068

Results relating to the rate of heat and mass transfers and the skin friction coefficients are obtained and presented in Table 4.2. Graphical results are obtained for the related profiles, momentum, thermal, and solutal boundary layers and discussed.

Table 4.2. Effects of control parameters on $-f''(0)$, $-\theta'(0)$ and $-\phi'(0)$

Pr	β	M	λ	Ec	Ra	Sc	S	$-\theta'(0)$	$-\phi'(0)$	$-f''(0)$
0.71	1.0	1	0.10	1.0	0.1	1	0.1	0.52200	0.96317	1.17621
5.00								1.4678	0.96317	1.17621
7.10								1.7221	0.96317	1.17621
0.71	2.0	1	0.10	1.0	0.1	1	0.1	0.50580	0.90968	1.36255
	3.0							0.49772	0.88496	1.44731
	4.0							0.49296	0.87065	1.49603
0.71	1.0	2	0.10	1.0	0.1	1	0.1	0.30088	0.89893	1.37689
		3						0.11908	0.84184	1.55106
		4						0.03689	0.78988	1.70716
0.71	1.0	1	0.22	1.0	0.1	1	0.1	0.52200	0.85804	1.17621
			0.24					0.52200	0.83565	1.17621
			0.26					0.52200	0.81041	1.17621
0.71	1.0	1	0.10	0.4	0.1	1	0.1	0.65904	0.96317	1.17621
				0.6				0.61336	0.96317	1.17621
				0.8				0.56768	0.96317	1.17621
0.71	1.0	1	0.10	1.0	0.2	1	0.1	0.48670	0.96317	1.17621
					0.3			0.45658	0.96317	1.17621
					0.4			0.43055	0.96317	1.17621
0.71	1.0	1	0.10	1.0	0.1	2	0.1	0.52200	1.53535	1.17621
						3		0.52200	1.98558	1.17621
						4		0.52200	2.37390	1.17621
0.71	1.0	1	0.10	1.0	0.1	1	0.2	0.56227	1.02724	1.20097

							0.3	0.60396	1.09341	1.22630
							0.4	0.64698	1.16156	1.25219

4.1. Numerical Results

The numerical results representing the effects of various controlling parameters on the heat and mass transfer rates and the skin-friction coefficient are presented in Table 4.2. It is noticed that the Prandtl number and the suction parameters contribute to raising the heat transfer rate from the surface. Conversely, the parameters, such as the Casson, the magnetic, the radiation, and the Eckert number, decrease the speed at which heat and mass are transferred from the surface, resulting in an increased skin-friction, which provides high resistance to the flow. It is further noted that the parameter of reaction rate caused a slowdown in the mass diffusion near the surface.

The radiation parameter decreases the rate of heat transfer from the surface, but the Schmidt number increases the mass transfer rate. It is interesting to know that both the radiation parameter and the Schmidt number do not influence the skin friction coefficient, along wth the flow speed. Suction is, however, observed to be an important control parameter as it leads to increases in the speed of heat or mass transfers and hence increases the skin friction coefficient, ultimately influencing the flow speed necessary for control cooling.

4.2. Graphical Results

The presentation of graphs of the effects of various controlling parameters on the concentration, temperature, and velocity profiles is illustrated. Figures 4.1 – 4.3 illustrates the velocity profiles for varying magnetic, suction, and Casson parameters, respectively.

4. Varying parameters for Velocity profiles

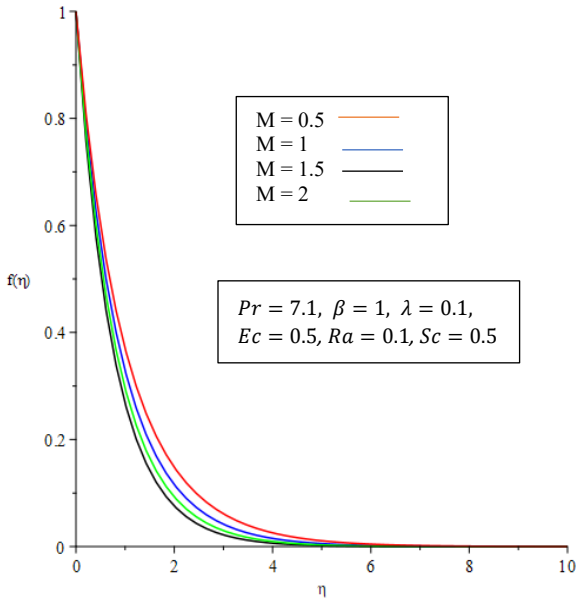

Fig 4.1. Magnetic(M) parameter effects on velocity

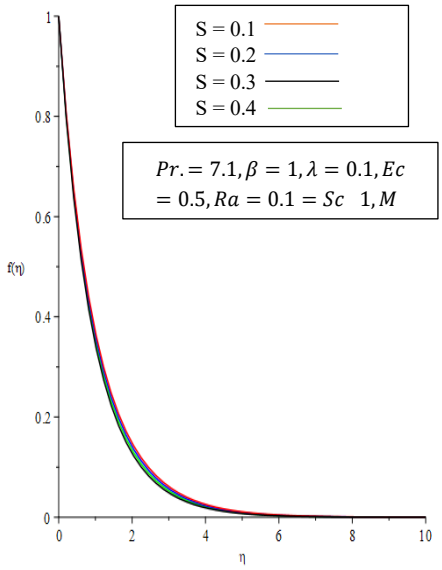

Fig 4.2. Suction parameter (S) effects

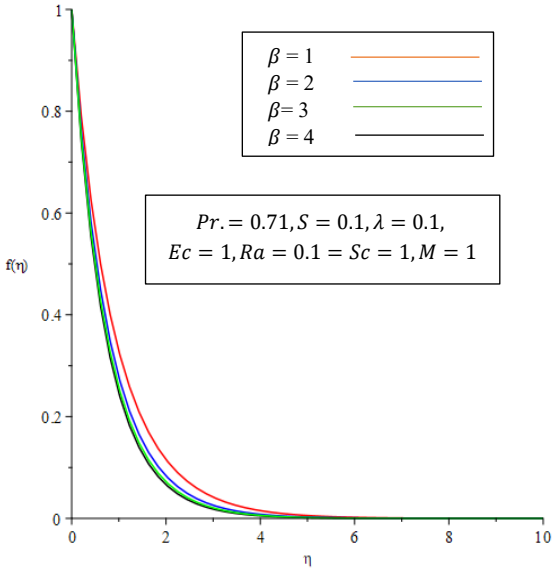

Fig 4.3. Effects of the parameter of Casson (β) on the velocity.

It is seen that increasing the magnetic parameter leads to a reduction in the velocity of the fluid, due to the presence of a drag-like force known as the Lorentz force. The motion of the fluid is opposed by this force, resulting in a slowdown in the overall velocity throughout the fluid domain (Figure 4.1). Figure 4.2 presents the suction effects on the velocity profile. It is observed that suction influences the velocity profile of the fluid flowing near a surface. Increasing the suction parameter lowers the velocity profiles, which makes the boundary layer of momentum thinner. Conversely, decreasing the suction parameter or injecting the fluid increases the velocity profile and thickens the boundary layer. Thus, understanding the effect of suction/injection on velocity profiles is important in many engineering applications, including aerodynamic flow control (e.g., preventing boundary layer separation on wings), heat transfer in porous media, and other fluid dynamic processes like metal extrusion.

In Figure 4.3, the Casson parameter effects on the fluid velocity are presented. Generally, increasing the Casson parameter brings about a reduction in the velocity profile of the fluid, effectively "slowing down" the flow. This is the result of the connection between the Casson parameter and the yield stress of the fluid, which is the stress required to initiate movement. As the parameter of Casson increases, the fluid exhibits a greater yield stress, making it more resistant to flow and therefore decreasing the velocity profile. Thus, the magnetic, suction, and Casson parameters are important parameters that can be used to influence the flow kinematics of the Casson fluids.

4.3 Temperature profiles for varying parameters

Figures 4.4 - 4.9 illustrate the effects of varying parameters on the thermal boundary layer thickness. Figure 4.4 highlights how the temperature profiles are affected by the magnetic field parameter. The parameter of the magnetic field contributes to the accumulation of heat in the flow, resulting in the thickening of the thermal boundary layer. It is a measurement of the fluid's interaction with a magnetic field and significantly impacts the flow and heat movement within the fluid. Increasing the magnetic parameter generally leads to higher temperature profiles as it reduces the fluid velocity and alters the heat movement mechanism. Conversely, the suction parameter, which controls the fluid flow in a system, significantly impacts the temperature profile. Increasing the suction parameter, particularly in a porous medium, leads to a decrease in heat flux and an increase in free surface temperature. This outcome results from the decrease in fluid velocity and heat transfer at the surface (Figure 4.5).

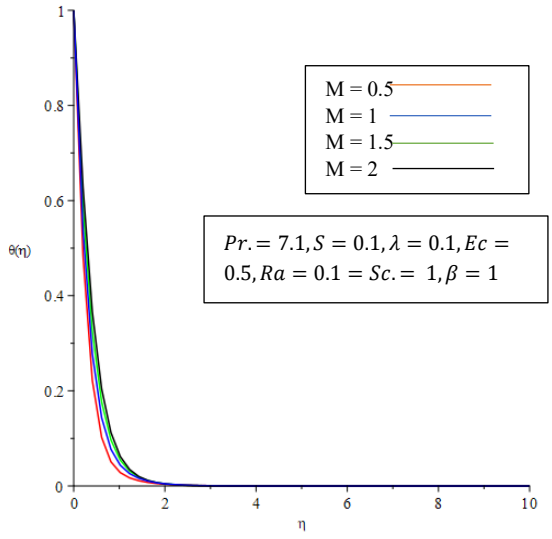

Fig. 4.4. Magnetic(M) parameter effects on temperature profile

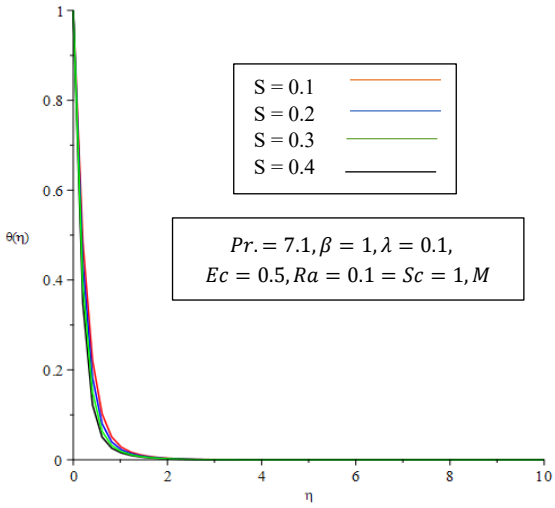

Fig 4.5. Suction parameter(S) effect on temperature profile

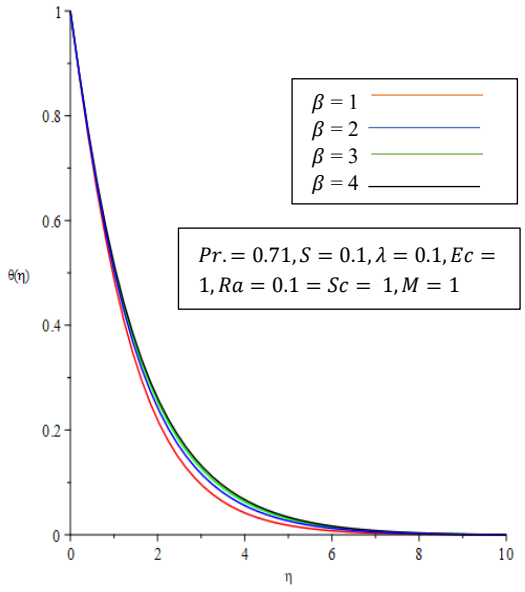

Fig. 4.6. Casson parameter effects on temperature profiles

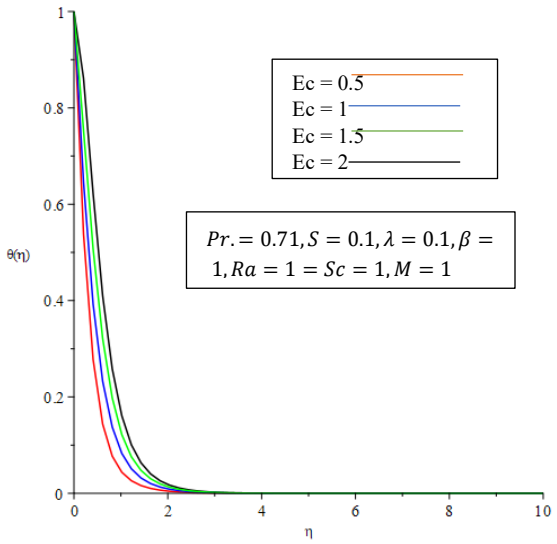

Fig. 4.7 Eckert number effects on temperature profiles

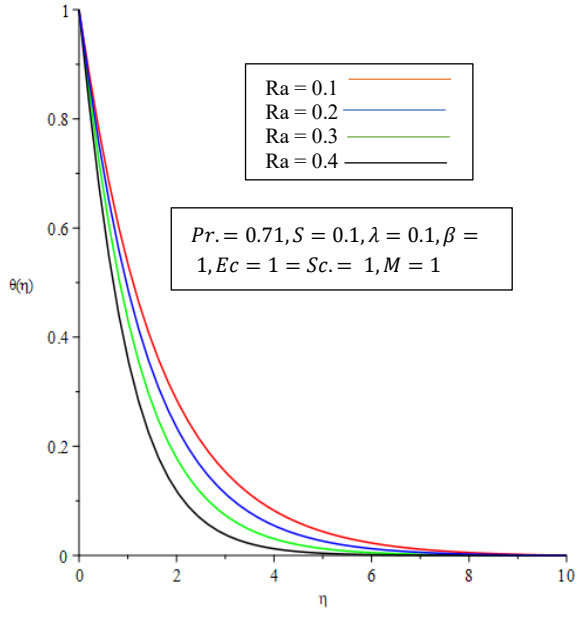

Fig. 4.8. Radiation parameter effects on temperature profile

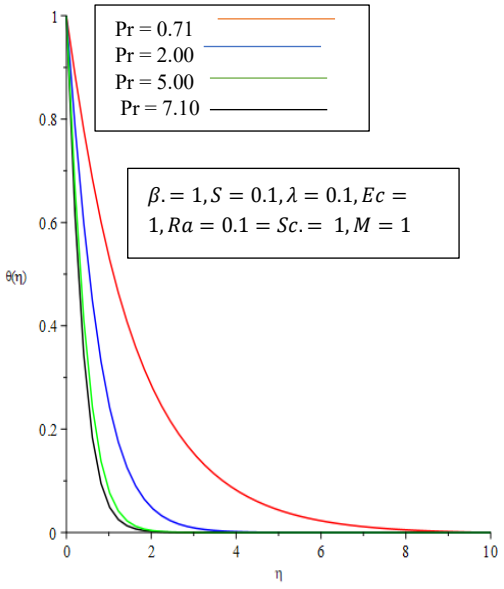

Fig. 4.9. Prandtl number effects on temperature profile

The Casson parameter (β) impacts the temperature profile by influencing the viscosity of the fluid and its ability to transfer heat. A higher Casson parameter (connoting a more non-Newtonian fluid) results in increased temperature profiles within the boundary layer. This effect is primarily due to the increased resistance to flow and the increased heat transfer associated with a larger Casson parameter (Figure 4.6).

Figure 4.7 illustrates the Eckert number (Ec) effects on the thermal boundary layer. The Eckert number describes the contribution of the kinetic energy of moving fluid to the overall temperature change. A higher Eckert number means a greater percentage of the fluid's kinetic energy is transformed into thermal energy due to dissipation of viscosity, leading to a hotter fluid. As such, a high Eckert number is associated with a rise in the temperature of the fluid.

The parameter of radiation(R) significantly impacts the temperature profile by influencing the amount of heat transferred through radiation. Increasing the parameter of radiation leads to a lower temperature within the fluid or the boundary layer (Figure 4.8). The Prandtl number (Pr) determines how quickly heat can diffuse through a fluid compared to momentum diffusion. A higher Prandtl indicates that less heat diffuses than momentum, leading to a thinner thermal boundary layer and potentially a steeper temperature gradient (Figure 4.9).

4.4. Concentration Profiles

Figures 4.10 – 4.14 present the graphical illustration for various control parameters such as the magnetic (M), the suction (S), the Casson (β) and the Schmidt number (Sc).

The parameter of magnetic (M) affects the concentration profile by influencing the velocity of the flow and the resulting temperature distribution. It generally leads to a decrease in velocity within

the boundary layer, and this decrease in velocity affects the diffusion of nanoparticles or other constituents in the fluid, ultimately impacting the concentration profile. The decrease in the velocity of the fluid affects the speed of diffusion of various substances within the fluid, including nanoparticles or other constituents. A slower flow rate leads to less mixing and potentially a more concentrated or stratified distribution of these substances (Figure 4.10).

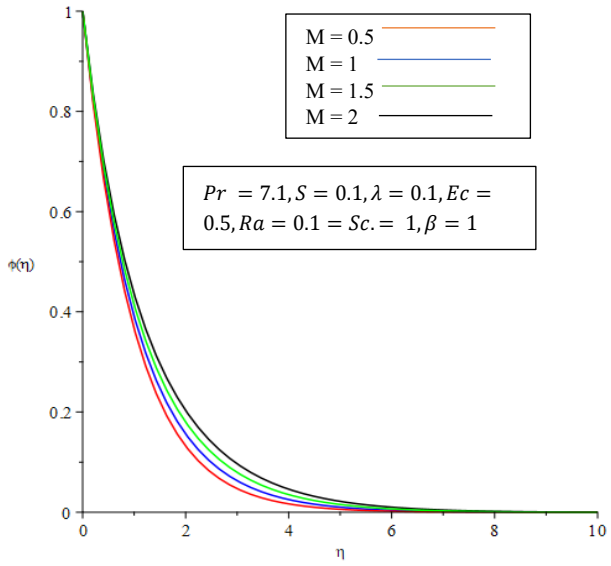

Fig 4.10. Magnetic parameter (M) effect on Concentration profile

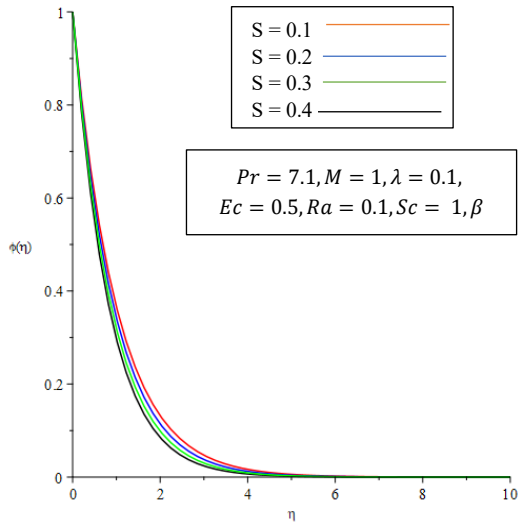

Fig 4.11. Suction parameter (S) effects on concentration profile

Figure 4.11 depicts the effect of suction on the boundary layer of concentration. The suction parameter (S) directly influences the concentration profile by altering the movement of the fluid and the rate at which species are transported across the boundary layer. Higher suction (S > 0) generally pulls the fluid closer to the wall, reducing the thickness of the concentration profile, and potentially leading to a decrease in concentration near the wall.

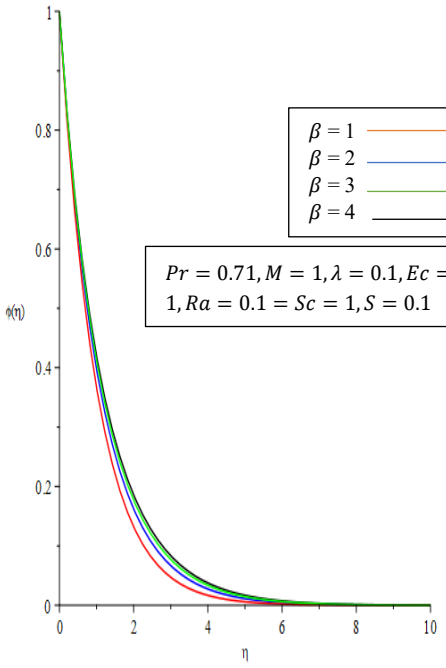

Fig 4.12. Casson parameter (β) effects on Concentration profile

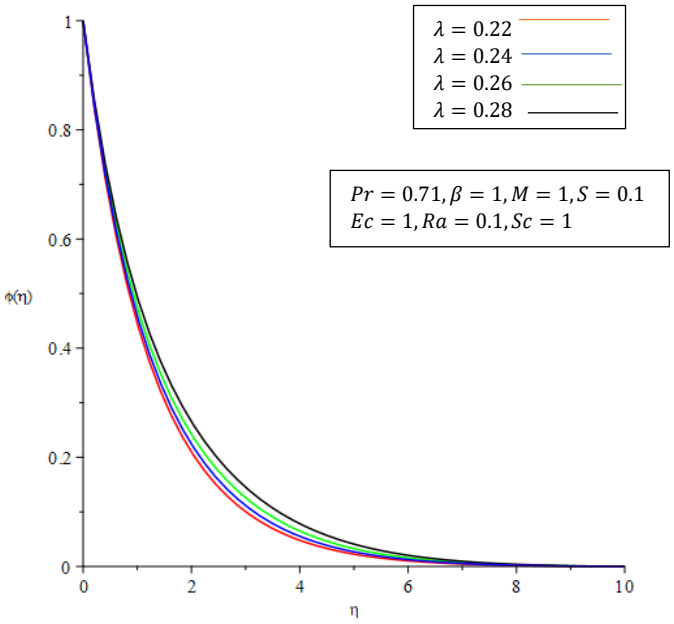

Fig 4.13. Reaction rate parameter (λ) effects on concentration profile

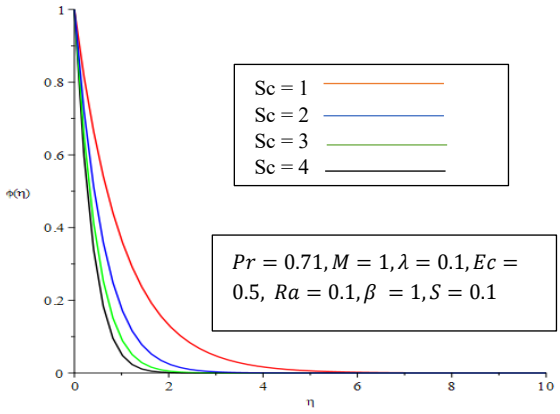

Fig 4.14. Schmidt number (Sc) effects on the concentration profile

The Casson parameter (β) significantly impacts concentration profiles by influencing the thickness and distribution of the concentration boundary layer, Figure 4.12. Higher Casson parameters

generally lead to an enlargement of the concentration boundary layer, meaning the concentration changes more rapidly near the surface. The parameter of the reaction rate (λ) directly influences the profile representing concentration by impacting the rate at which reactants are consumed and products are formed, as shown in Figure 4.13. A higher reaction rate parameter indicates a faster reaction, leading to a thinner concentration boundary layer and a more rapid decrease in reactant concentration near the surface. Conversely, a lower reaction rate parameter suggests a slower reaction, resulting in a boundary layer concentration being thicker and a slower depletion of reactants.

The Schmidt number (Sc) relates the momentum diffusivity to the mass diffusivity in a fluid. It provides a measure of how readily a solute is transported by diffusion compared to its transport by fluid motion. A higher Schmidt number indicates that the concentration boundary layer is thinner relative to the velocity boundary layer, meaning the concentration profile is more strongly affected by fluid motion and less by diffusion. The effects of the Schmidt number on the concentration boundary layer are depicted in Figure 4.14. It is observed that increasing the value of the Schmidt number reduces the concentration boundary layer due to the deposition of reactive elements in the flow field.

CHAPTER FIVE
CONCLUSION AND RECOMMENDATIONS

5.0. Introduction

In this research, Casson fluid flow on a porous medium with exponential stretching in the existence of a transverse magnetic field and chemical reaction has been presented. It is observed from the study that the parameter of Casson, the parameter of thermal radiation, and the parameters of the magnetic field significantly influence the flow and heat transfer characteristics. The following conclusions are made:

5.1. Conclusions

- Increased parameter of Casson suppresses the velocity field but enhances the thermal boundary layer. The Casson parameter is an important factor influencing fluid kinematics, affecting both velocity and temperature.
- Increasing the parameter of the magnetic field results in a high induced Lorentz force, which impedes the fluid velocity, resulting in increased thermal and concentration boundary layers.
- High Casson parameter and parameter of magnetic field result in increased skin friction and heat transfer rates, which are relevant to various applications, including blood flow modelling and drag reduction in industrial processes.
- Thermal radiation has the effect of enhancing thermal diffusivity, resulting in increased temperature of the fluid.
- Suction parameter has the effect of drawing fluid into the surface, resulting in enhanced skin friction, which causes a reduction in the velocity of flow.

- Chemical reaction within the fluid influences mass transfer rates and concentration profiles.

5.2. Recommendations

In this research, the study is based on two-dimensional steady incompressible flow for non-Newtonian fluids, taking into consideration only Casson fluids. It can be expanded into the following:

- By extending the model to include nanofluids by incorporating Brownian motion and thermophoresis parameters.
- Extend the model to account for unsteady (time-dependent) flow
- Introduce temperature or concentration-dependent viscosity, thermal conductivity, and diffusivity.
- Finally, the developed model can be applied to practical systems such as magnetic drug delivery, heat management in porous reactors, and polymer extrusions. It is suggested that future studies focus on validating such applications in industrial case studies.

References

Ahmad, Z., Crisci, S., Murtaza, S., & Toraldo, G. (2024). Numerical insights of fractal–fractional modeling of magnetohydrodynamic Casson hybrid nanofluid with heat transfer enhancement. *Mathematical Methods in the Applied Sciences*.

Ahmadi Azar, A., Jalili, P., Jalili, B., & Ganji, D. D. (2024). The comprehensive analysis of magnetohydrodynamic Casson fluid flow with rectangular porous medium through expanding/contracting channel. *Multidiscipline Modeling in Materials and Structures*.

Akaje, W. T. (2021). Stagnation point heat flow and mass transfer in a Casson nanofluid with viscous dissipation and inclined magnetic field. *UKH Journal of Science and Engineering*, *5*(1), 38–49.

Aloliga, G., Seini, I. Y., & Musah, R. (2022). *On Hydromagnetic Boundary Layer of Casson Fluid Over Porous Inclined Magnetized Surface With Radiation and Convective Boundary Conditions*.

Archana, M., Gireesha, B. J., Prasannakumara, B. C., & Gorla, R. S. R. (2018). Influence of nonlinear thermal radiation on rotating flow of Casson nanofluid. *Nonlinear Engineering*, *7*(2), 91–101.

Bau, H. H. (2022). Applications of magneto electrochemistry and magnetohydrodynamics in microfluidics. *Magnetochemistry*, *8*(11), 140.

Bera, T. K. (2020). A magnetohydrodynamic (MHD) power generating system: a technical

review. *IOP Conference Series: Materials Science and Engineering*, *955*(1), 12075.

Bergman, T. L. (2011). *Fundamentals of heat and mass transfer*. John Wiley & Sons.

Blasius, H. (1908). The Boundary Layers in Fluids. *Zeitschrift Fixr Mathematik Und Physik*, *56*(1).

Bluman, G. W., & Cole, J. D. (2012). *Similarity methods for differential equations* (Vol. 13). Springer Science & Business Media.

Casson, N. (1959). Flow equation for pigment-oil suspensions of the printing ink-type. *Rheology of Disperse Systems*, 84–104.

Cess, R. D. (1964). The interaction of thermal radiation with conduction and convection heat transfer. In *Advances in heat transfer* (Vol. 1, pp. 1–50). Elsevier.

Chhabra, R. P., & Richardson, J. F. (2011). *Non-Newtonian flow and applied rheology: engineering applications*. Butterworth-Heinemann.

Clough, K. (2021). Continuity equations for general matter: applications in numerical relativity. *Classical and Quantum Gravity*, *38*(16), 167001.

Crane, L. J. (1970). Flow past a stretching plate. *Zeitschrift Für Angewandte Mathematik Und Physik ZAMP*, *21*, 645–647.

Cussler, E. L. (2009). *Diffusion: mass transfer in fluid systems*. Cambridge university press.

Dang, K., Makkar, V., & Sharma, N. (2021). Numerical analysis of three-dimensional magnetohydrodynamics non-Newtonian free stream flow induced by permeable stretching surface. *Journal of Thermal Engineering*, *10*(6), 1465–1479.

Dey, D., Borah, R., & Makinde, O. D. (2023). Free Convection of a Radiating MHD Nanofluid Past a Solid Sphere with Energy Transfer in a Porous Medium. *International Journal of Applied and Computational Mathematics*, *9*(6), 143.

Dhlamini, M., Zondo, K., Duve, P., Mondal, H., Mishra, S., Sibanda, P., Shaw, S., & Motsa, S. (2024). Cattaneo-Christov heat flux-based micropolar nanofluid flow with relaxation, slip, and temperature jump effects. *Results in Engineering*, 102645.

Epifanov, V. M. (2011). Boundary layer. In *Thermopedia*. Begel House Inc.

Esmaeili, E. (2022). *Squeeze film flow of viscoplastic Bingham fluids*.

Faraz, F., Haider, S., & Imran, S. M. (2020). Study of magneto-hydrodynamics (MHD) impacts on an axisymmetric Casson nanofluid flow and heat transfer over unsteady radially stretching sheet. *SN Applied Sciences*, *2*, 1–17.

Farooq, U., Hayat, T., Alsaedi, A., & Liao, S. J. (2015). Series solutions of non-similarity boundary layer flows of nano-fluids over stretching surfaces. *Numerical Algorithms*, *70*, 43–59.

Franco, J. M., & Partal, P. (2010). The newtonian fluid. *Rheology*, *1*, 74–95.

Glicksman, M. (2020). Functional properties of hydrocolloids. In *Food hydrocolloids* (pp. 47–99). CRC Press.

Haugan, M. P. (1979). Energy conservation and the principle of equivalence. *Annals of Physics*, *118*(1), 156–186.

Hazarika, G. C., & Konch, J. (2014). Effects of Variable viscosity and thermal conductivity on MHD free convective flow along a vertical porous plate with viscous dissipation.

International Journal of Mathematics Trends and Technology-IJMTT, *15*.

Irgens, F. (2014). *Rheology and non-newtonian fluids* (Vol. 1). Springer.

Islam, R., Hossain, A., Biswas, R., Hasan, M., Rana, B. M. J., Habibullah, H., & Afikuzzaman, M. (2025). Modelling and theoretical overview of Casson fluid flow through a stretching sheet with variable viscosity and sinusoidal boundary conditions. *International Journal of Ambient Energy*, *46*(1), 2539139.

Jamshed, W., Mohd Nasir, N. A. A., Brahmia, A., Nisar, K. S., & Eid, M. R. (2022). Entropy analysis of radiative [MgZn6Zr-Cu/EO] Casson hybrid nanoliquid with variant thermal conductivity along a stretching surface: Implementing Keller box method. *Proceedings of the Institution of Mechanical Engineers, Part C: Journal of Mechanical Engineering Science*, *236*(12), 6501–6520.

Khan, M. I., Alsaedi, A., Hayat, T., & Khan, N. B. (2019). Modeling and computational analysis of hybrid class nanomaterials subject to entropy generation. *Computer Methods and Programs in Biomedicine*, *179*, 104973.

Koka, R., & Ganjikunta, A. (2024). Effect of the Aligned Magnetic Field over a Stretching Sheet through Porous Media in Casson Fluid Flow. *CFD Letters*, *16*(4), 16–38.

Kumar, S., & Pai, N. (2020). Flow of casson fluid through circular porous bearing. *CFD Letters*, *12*(7), 48.

Leelavathi, R., Vyakaranam, S., Rao, T. S., Gurrampati, V. R. R., & Oke, A. S. (2024). MHD Casson Fluid Flow in Stagnation-Point over an Inclined Porous Surface. *CFD Letters*, *16*(4), 69–84.

Liu, P. (2022). Boundary Layer Theory and Its Approximation. In *Aerodynamics* (pp. 307–393). Springer.

Makkar, V., Dang, K., Sharma, N., & Yadav, S. (2023). Numerical investigation of MHD convective free stream nanofluid flow influenced by radiation and chemical reaction over stretching cylinder. *Heat Transfer*, *52*(3), 2328–2347.

Mini, G. S., Kumar, P. V., & Shaik, M. I. (2024). Numerical Simulations of Chemically Dissipative MHD Mixed Convective Non-Newtonian Nanofluid Stagnation Point Flow over an Inclined Stretching Sheet with Thermal Radiation Effects. *CFD Letters*, *16*(5), 37–58.

Miyan, M. (2018). Analysis on the MHD Power Generation Technology. *World Wide Journal of Multidisciplinary Research and Development*, *4*, 309–313.

Moktarian, F., & Modi, V. J. (1988). Fluid dynamics of airfoils with moving surface boundary-layer control. *Journal of Aircraft*, *25*(2), 163–169.

Nguyen, Q.-H., & Nguyen, N.-D. (2012). Incompressible non-Newtonian fluid flows. *Continuum Mechanics-Progress in Fundamentals and Engineering Applications*, *1*, 47–72.

Noor, N. A. M., Mahadi, S., Nordin, N. S., Arbin, N., Shafie, S., Admon, M. A., & Jiann, L. Y. (2024). Squeezing MHD Flow of Sodium Alginate-Based Casson Hybrid Nanofluid with Soret and Dufour Effects. *Journal of Advanced Research in Fluid Mechanics and Thermal Sciences*, *116*(1), 97–115.

Norasia, Y., Tafrikan, M., Ghani, M., Asmianto, A., & Anggriani, I. (2023). Study of The Effect Stuart and Prandtl Numbers on Diamond Nano Fluid Flowing Through Cylindrical Surface. *Telematika*, *16*(1), 12–24.

Pal, D., & Talukdar, B. (2010). Buoyancy and chemical reaction effects on MHD mixed convection heat and mass transfer in a porous medium with thermal radiation and Ohmic heating. *Communications in Nonlinear Science and Numerical Simulation*, *15*(10), 2878–2893.

Pramanik, S. (2014). Casson fluid flow and heat transfer past an exponentially porous stretching surface in presence of thermal radiation. *Ain Shams Engineering Journal*, *5*(1), 205–212.

Prandtl, L. (1905). Uber Flussigkeitsbewegung bei sehr kleiner Reibung. *Verhandl. 3rd Int. Math. Kongr. Heidelberg (1904), Leipzig*.

Price, D. (2012). Shear-Thickening Fluid. *Physics Department, The College of Wooster*, 1–4.

Priest, E. R. (1982). The basic equations of magnetohydrodynamics. In *Solar Magnetohydrodynamics* (pp. 73–116). Springer.

Ramana Reddy, G. V., & Chamkha, A. J. (2015). Lie group analysis of chemical reaction effects on MHD free convection dissipative fluid flow past an inclined porous surface. *International Journal of Numerical Methods for Heat & Fluid Flow*, *25*(7), 1557–1573.

Rao, M. A. (1995). Rheological properties of fluid foods. *FOOD SCIENCE AND TECHNOLOGY-NEW YORK-MARCEL DEKKER-*, 1.

Reddy, M. G., Reddy, K. V., & Makinde, O. D. (2016). Hydromagnetic peristaltic motion of a reacting and radiating couple stress fluid in an inclined asymmetric channel filled with a porous medium. *Alexandria Engineering Journal*, *55*(2), 1841–1853.

Saidulu, N., & Lakshmi, A. V. (2016). MHD flow of Casson fluid with slip effects over an exponentially porous stretching sheet in presence of thermal radiation, viscous dissipation

and heat source/sink. *American Research J. of Mathematics*, *2*(1), 1–15.

Sakiadis, B. C. (1961). Boundary-layer behavior on continuous solid surfaces: I. Boundary-layer equations for two-dimensional and axisymmetric flow. *AIChE Journal*, *7*(1), 26–28.

Sawlat, N., Qani, Y., & Sadeqi, N. (2024). Numerical and Symbolic Analysis for Mathematical Problem-Solving with Maple. *Journal of Natural Science Review*, *2*(3), 29–46.

Seini, I. Y. (2019). Heat and mass transfer from a convectively heated vertical surface with chemical reaction and internal heat generation. *Engineering Transactions*, *67*(1), 101–118.

Seini, I. Y., Aloliga, G., Ziblim, B., & Makinde, O. D. (2020). Boundary layer flow of casson fluid on exponentially stretching porous surface with radiative heat transfer. *Diffusion Foundations*, *26*, 112–125.

Seuss, D. (1949). Bartholomew and the Oobleck. *(No Title)*.

Sharma, A. (2021). Newton's generalized form of second law gives F= ma. *IOSR Journal Of Applied Physics*, *13*(2), 61–137.

Sulemana, M., Seini, I. Y., & Makinde, O. D. (2022). *Research Article Hydrodynamic Boundary Layer Flow of Chemically Reactive Fluid over Exponentially Stretching Vertical Surface with Transverse Magnetic Field in Unsteady Porous Medium*.

Sushma, S., & Gireesha, B. J. (2024). *A Comprehensive Study of Nonlinear Stretching Sheet in Stagnation Point Flow of Casson Fluid: Unveiling New Similarity Transformations*.

Talla, H. (2020). Numerical Study of MHD flow and Heat Transfer over an exponentially permeable stretching Surface of Casson Fluid.*International Journal of Mechanical Production Engineering Research and Department*,2457-2464.

Uddin, Z., Upreti, H., Ganga, S., & Ibrahim, W. (2024). Particle Swarm Optimization for exploring Darcy–Forchheimer flow of Casson fluid between co-axial rotating disks with the Cattaneo–Christov model. *Scientific Reports*, *14*(1), 7891.

White, F. M., & Majdalani, J. (2006). *Viscous fluid flow* (Vol. 3). McGraw-Hill New York.

Yashkun, U., Lund, L. A., Fadhel, M. A., & Shah, N. A. (2024). Velocity slip effect on magnetized casson nanofluid over shrinking/stretching cylinder: duality and stability analysis. *Physica Scripta*, *99*(2), 25203.

Appendix

Graphical codes

```
with(plots);

Pr := 0.71;

beta := 1;

M := 1;

lambda := 0.1;

Ec := 1;

Ra := 0.1;

Sc := 1;

S := 0.1;

fcns := {F(y), phi(y), theta(y)};

sys := (1 + 1/beta)*diff(F(y), y $ 3) + F(y)*diff(F(y), y $ 2) - 2*diff(F(y), y)^2 - M*diff(F(y), y) = 0, (1 - 4/3*Ra)*diff(theta(y), y $ 2) + Pr*F(y)*diff(theta(y), y) - Pr*diff(F(y), y)*theta(y) + Pr*M*Ec*diff(F(y), y)^2 = 0, diff(phi(y), y $ 2) + Sc*F(y)*diff(phi(y), y) - Sc*diff(F(y), y)*phi(y) + Sc*lambda*phi(y);

p1 := dsolve({sys, F(0) = S, phi(0) = 1, phi(10) = 0, theta(0) = 1, theta(10) = 0, D(F)(0) = 1, D(F)(10) = 0}, fcns, type = numeric, method = bvp, abserr = 0.1e-5);

p1t := odeplot(p1, [y, theta(y)], 0 .. 10, numpoints = 50, labels = ["&eta;", "&theta;(&eta;)"], style = line, symbol = point, color = red);

p1f := odeplot(p1, [y, D(F)(y)], 0 .. 10, numpoints = 50, labels = ["&eta;", "f(&eta;)"], style = line, symbol = point, color = red);

p1c := odeplot(p1, [y, phi(y)], 0 .. 10, numpoints = 50, labels = ["&eta;", "&phi;(&eta;)"], style = line, symbol = point, color = red);
```

```
with(plots);

Pr := 0.71;

beta := 1;

M := 2;

lambda := 0.1;

Ec := 1;

Ra := 0.1;

Sc := 1;

S := 0.1;

fcns := {F(y), phi(y), theta(y)};

sys := (1 + 1/beta)*diff(F(y), y $ 3) + F(y)*diff(F(y), y $ 2) - 2*diff(F(y), y)^2 - M*diff(F(y), y) = 0, (1 -
4/3*Ra)*diff(theta(y), y $ 2) + Pr*F(y)*diff(theta(y), y) - Pr*diff(F(y), y)*theta(y) + Pr*M*Ec*diff(F(y),
y)^2 = 0, diff(phi(y), y $ 2) + Sc*F(y)*diff(phi(y), y) - Sc*diff(F(y), y)*phi(y) + Sc*lambda*phi(y);


p2 := dsolve({sys, F(0) = S, phi(0) = 1, phi(10) = 0, theta(0) = 1, theta(10) = 0, D(F)(0) = 1, D(F)(10) = 0},
fcns, type = numeric, method = bvp, abserr = 0.1e-5);

p2t := odeplot(p2, [y, theta(y)], 0 .. 10, numpoints = 50, labels = ["&eta;", "&theta;(&eta;)"], style = line,
symbol = point, color = blue);

p2f := odeplot(p2, [y, D(F)(y)], 0 .. 10, numpoints = 50, labels = ["&eta;", "f(&eta;)"], style = line, symbol =
point, color = blue);

p2c := odeplot(p2, [y, phi(y)], 0 .. 10, numpoints = 50, labels = ["&eta;", "&phi;(&eta;)"], style = line,
symbol = point, color = blue);




with(plots);

Pr := 0.71;

beta := 1;

M := 3;

lambda := 0.1;
```

```
Ec := 1;

Ra := 0.1;

Sc := 1;

S := 0.1;

fcns := {F(y), phi(y), theta(y)};

sys := (1 + 1/beta)*diff(F(y), y $ 3) + F(y)*diff(F(y), y $ 2) - 2*diff(F(y), y)^2 - M*diff(F(y), y) = 0, (1 - 4/3*Ra)*diff(theta(y), y $ 2) + Pr*F(y)*diff(theta(y), y) - Pr*diff(F(y), y)*theta(y) + Pr*M*Ec*diff(F(y), y)^2 = 0, diff(phi(y), y $ 2) + Sc*F(y)*diff(phi(y), y) - Sc*diff(F(y), y)*phi(y) + Sc*lambda*phi(y);


p3 := dsolve({sys, F(0) = S, phi(0) = 1, phi(10) = 0, theta(0) = 1, theta(10) = 0, D(F)(0) = 1, D(F)(10) = 0}, fcns, type = numeric, method = bvp, abserr = 0.1e-5);

p3t := odeplot(p3, [y, theta(y)], 0 .. 10, numpoints = 50, labels = ["&eta;", "&theta;(&eta;)"], style = line, symbol = point, color = green);

p3f := odeplot(p3, [y, D(F)(y)], 0 .. 10, numpoints = 50, labels = ["&eta;", "f(&eta;)"], style = line, symbol = point, color = green);

p3c := odeplot(p3, [y, phi(y)], 0 .. 10, numpoints = 50, labels = ["&eta;", "&phi;(&eta;)"], style = line, symbol = point, color = green);
```


```
with(plots);

Pr := 0.71;

beta := 1;

M := 4;

lambda := 0.1;

Ec := 1;

Ra := 0.1;

Sc := 1;

S := 0.1;

fcns := {F(y), phi(y), theta(y)};
```

```
sys := (1 + 1/beta)*diff(F(y), y $ 3) + F(y)*diff(F(y), y $ 2) - 2*diff(F(y), y)^2 - M*diff(F(y), y) = 0, (1 - 4/3*Ra)*diff(theta(y), y $ 2) + Pr*F(y)*diff(theta(y), y) - Pr*diff(F(y), y)*theta(y) + Pr*M*Ec*diff(F(y), y)^2 = 0, diff(phi(y), y $ 2) + Sc*F(y)*diff(phi(y), y) - Sc*diff(F(y), y)*phi(y) + Sc*lambda*phi(y);


p4 := dsolve({sys, F(0) = S, phi(0) = 1, phi(10) = 0, theta(0) = 1, theta(10) = 0, D(F)(0) = 1, D(F)(10) = 0}, fcns, type = numeric, method = bvp, abserr = 0.1e-5);

p4t := odeplot(p4, [y, theta(y)], 0 .. 10, numpoints = 50, labels = ["&eta;", "&theta;(&eta;)"], style = line, symbol = point, color = black);

p4f := odeplot(p4, [y, D(F)(y)], 0 .. 10, numpoints = 50, labels = ["&eta;", "f(&eta;)"], style = line, symbol = point, color = black);

p4c := odeplot(p4, [y, phi(y)], 0 .. 10, numpoints = 50, labels = ["&eta;", "&phi;(&eta;)"], style = line, symbol = point, color = black);
```

Numerical codes

```
Pr := 0.71;

beta := 1;

M := 2;

lambda := 0.1;

Ec := 1;

Ra := 0.1;

Sc := 1;

S := 0.1;

fcns := {F(y), phi(y), theta(y)};

sys1 := (1 + 1/beta)*diff(F(y), y $ 3) + F(y)*diff(F(y), y $ 2) - 2*diff(F(y), y)^2 - M*diff(F(y), y) = 0, (1 - 4/3*Ra)*diff(theta(y), y $ 2) + Pr*F(y)*diff(theta(y), y) - Pr*diff(F(y), y)*theta(y) + Pr*M*Ec*diff(F(y), y)^2 = 0, diff(phi(y), y $ 2) + Sc*F(y)*diff(phi(y), y) - Sc*diff(F(y), y)*phi(y)
```

+ Sc*lambda*phi(y) = 0, D(F)(0) = 1, F(0) = S, theta(0) = 1, phi(0) = 1, D(F)(10) = 0, theta(10) = 0, phi(10) = 0;

dsol1 := dsolve({sys1}, numeric, output = operator);